UCRL-16288

University of California

Ernest O. Lawrence Radiation Laboratory

K^-p CHARGE-EXCHANGE SCATTERING FROM 1200 TO 1700 MeV/c

Berkeley, California

DISCLAIMER

Research and Development

UCRL-16288

UNIVERSITY OF CALIFORNIA

Lawrence Radiation Laboratory
Berkeley, California

Contract No. W-7405-eng-48

K^-p CHARGE-EXCHANGE SCATTERING FROM 1200 TO 1700 MeV/c

Charles Gordon Wohl

(Ph. D. Thesis)

July 13, 1965

K^-p CHARGE-EXCHANGE SCATTERING FROM 1200 TO 1700 MeV/c

Contents

K^-p CHARGE-EXCHANGE SCATTERING FROM 1200 TO 1700 MeV/c

Charles Gordon Wohl

Lawrence Radiation Laboratory
University of California
Berkeley, California

July 13, 1965

ABSTRACT

The Lawrence Radiation Laboratory's 72-inch hydrogen bubble chamber was exposed to a beam of K^- mesons having laboratory momenta of 1.22, 1.42, 1.51, 1.60, and 1.70 BeV/c. The K^-p charge-exchange-scattering differential cross sections were measured. The cross sections are, from low to high momentum, 2.83 ± 0.14, 1.90 ± 0.12, 1.83 ± 0.09, 1.93 ± 0.13, and 1.66 ± 0.10 mb. The differential cross sections are peaked at the ends ($\cos\theta = \pm 1$); there are two intermediate maxima. As the momentum increases, the peaking shifts rapidly from the backward to the forward direction. Though the forward (low-momentum-transfer) peaking at the higher momenta is considerable, a peripheral mechanism is by itself insufficient to reproduce the angular distribution. The differential cross sections are fit to Legendre polynomial series. At 1.22 BeV/c, the series including $P_6(\cos\theta)$ is necessary and sufficient; at the higher momenta, $P_7(\cos\theta)$ is required. The $F_{7/2}$ and $G_{7/2}$ partial-wave amplitudes are both present. At 1.60 and 1.70 BeV/c, the $J = 7/2$ partial waves account for at least a third of the cross section. The behavior as a function of energy of some of the coefficients of the Legendre-polynomial expansion suggests, though does not definitely establish, the existence of an $F_{7/2}$ $Y_1^*(2065)$. This has the quantum numbers of the recurrence of the $Y_1^*(1385)$ and belongs to the decuplet containing the $N_{3/2}^*(1920)$.

I. INTRODUCTION

The experiment was performed at the Lawrence Radiation Laboratory's Bevatron. The 72-inch hydrogen bubble chamber was exposed to a beam of K^- mesons having laboratory (lab) momenta between 1.20 and 1.70 BeV/c. About 30 000 events consisting of a disappearing beam track and an associated charged decay of a neutral particle were found. After kinematic analysis and application of further selection criteria, there remained 14 173 Λ events ($\Lambda \rightarrow p + \pi^-$) and 8408 $\overline{K}^0$ events ($K_1^0 \rightarrow \pi^+ + \pi^-$). Results of the analysis of the Λ events will be presented in a subsequent paper.[1] Here the subject is the $\overline{K}^0$ events, particularly the approximately 50% of them that are charge-exchange scatters, $K^- + p \rightarrow \overline{K}^0 + n$.[2]

Section II discusses briefly general experimental procedure--the characteristics of the beam, the scanning and measuring of events, and the computer programs that process the measurements. This assembly line for production of physics data varies little from one bubble chamber experiment to another.[3] Accordingly, only those aspects of particular relevance are discussed.

Section III contains the treatment of the data. The kinematic analysis, the various criteria imposed on the events in order to minimize biases, the methods of correcting for remaining biases, and the path-length determination are dealt with in turn. Results of the analysis, the total and differential charge-exchange-scattering cross sections, are presented in Section IV. The angular distributions are fit to Legendre-polynomial series.

Finally, in Section V, the implications of the results are investigated. A peripheral mechanism is insufficient to reproduce the angular distributions. An analysis of the coefficients of the Legendre-polynomial expansions establishes the importance of the $J = 7/2$ partial-wave amplitudes throughout the region of the experiment. The possible existence of a $J = 7/2$ Y^* resonant state is discussed. Comparison is made with predictions of the SU(3) and Regge trajectory schemes.

II. EXPERIMENTAL METHOD

A. Beam

The beam was designed to obtain K^- mesons at any laboratory momentum from 1.20 to 1.95 BeV/c. Negative particles, produced in a target flipped into the Bevatron's narrow circulating proton beam, were bent outward by the Bevatron's magnetic field and steered into the beam channel. The central momentum of the particles entering the channel was determined largely by the target position. A moveable target was required in order to vary the momentum over such a wide range.

The beam layout is shown in Fig. 1. It consisted of two similar stages, each with a crossed electric- and magnetic-field spectrometer, followed by a narrow horizontal slit. The spectrometers passed without vertical deflection only those particles having the velocity of a K^- with the desired momentum. Combined with momentum selection, this made a filter which passed K^- mesons but rejected other mass components. Magnets in the beam line acted as focusing elements. Extensive magnet shimming was done to correct for chromatic and nonlinear optical distortions of target and slit images.

The initially much more copius π flux was reduced by a factor 10^5. In the same way, the μ flux, resulting from the decay of particles in the beam line, was largely eliminated. At the bubble chamber, the π and μ contaminations were each about 5%.[4] The observed number of associated-production processes, $\pi^- + p \rightarrow K^0 + \Lambda$ (with visible decays) indicates that about 20 events of the type $\pi^- + p \rightarrow K^0 +$ neutrals (with visible K^0 decay) occur in the data. This is to be compared with a total of more than 8000 $\overline{K}^0$ events; the contamination is therefore completely negligible. The μ mesons do not contribute to the $\overline{K}^0$ topology. The K^- path length was obtained from a count of events with a topology unique to K^- decay, rather than by direct measurement of beam track length through the chamber.

Exposures were taken at approximately every 100 MeV/c. The momentum bite in each case was about 6% full width. By far the most

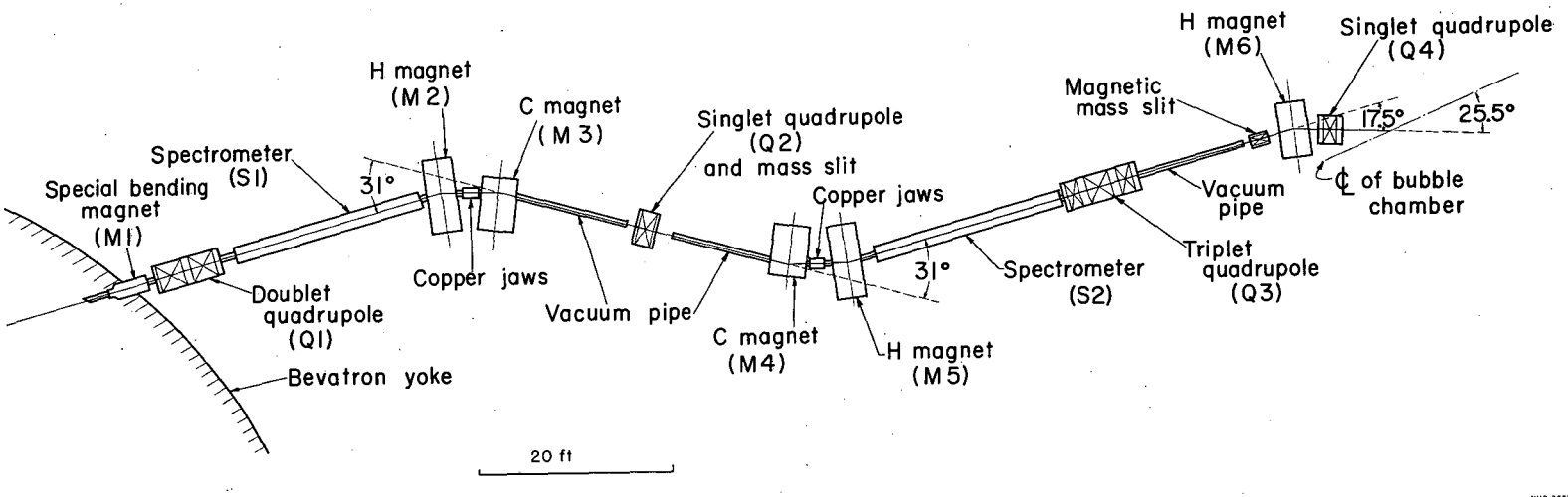

Fig. 1. Beam layout. The target (not shown) is the optical object for the first separation stage, which extends from the steering magnet M1 to the slit inside of quadrupole Q2. The first slit is the object for the second separation stage, which extends to the slit immediately in front of the magnet M6. The bubble chamber sees the image of the second slit.

film was taken at 1.51 BeV/c. Figure 2 is the beam-momentum spectrum of 8408 events in which $\overline{K}^0$'s are produced. The momentum settings were 1.22, 1.42, 1.51, 1.60, and 1.70 BeV/c. (Data at 1.33 BeV/c were analyzed at the University of Illinois, data at 1.80 and 1.95 BeV/c at UCLA; see below.) Since the cross section for $\overline{K}^0$ production is approximately constant over the range of momenta, the histogram reflects the relative amounts of data accumulated at the various momenta. About 3.3×10^5 pictures (of three views each) were taken. The K^- path length is conveniently specified by the number of events that would occur for a reaction channel having a cross section of 1 mb; after fairly severe fiducial criteria were imposed (Sec. III. B), the total path length was 7500 events/mb.

B. Scanning

The topologies of concern here, as they appear in the bubble chamber, are shown in Fig. 3. A charge-exchange reaction (as well as other reactions) appears as a vanishing beam track (0-prong) and a V-like decay which points back at the production vertex. The V can be either upstream or down from the 0-prong. See Fig. 4. The 3-prongs are a configuration that result only from certain K^- decay modes; their number provides a measure of the K^- path length.

All film was scanned twice for all topologies except 0-, 1-, and 2-prong events. To the extent described below, discrepancies between the two scans were re-examined and resolved on the scan table. Otherwise the first scan provided the list of events. This "master list", punched on cards and transferred to magnetic tape, contained scan data such as roll, frame, topology, and approximate chamber coordinates for each event; it served as a "bookkeeper" for the measuring.

The film at 1.22 BeV/c was the first to be taken. About 20% of it was not used because the quality was poor. In addition, the initial scan of this film was of low efficiency; eventually two scans of the V 0-prong events and three scans of the 3-prong events were compared and resolved. The exposures at 1.42 and 1.60 BeV/c were the smallest,

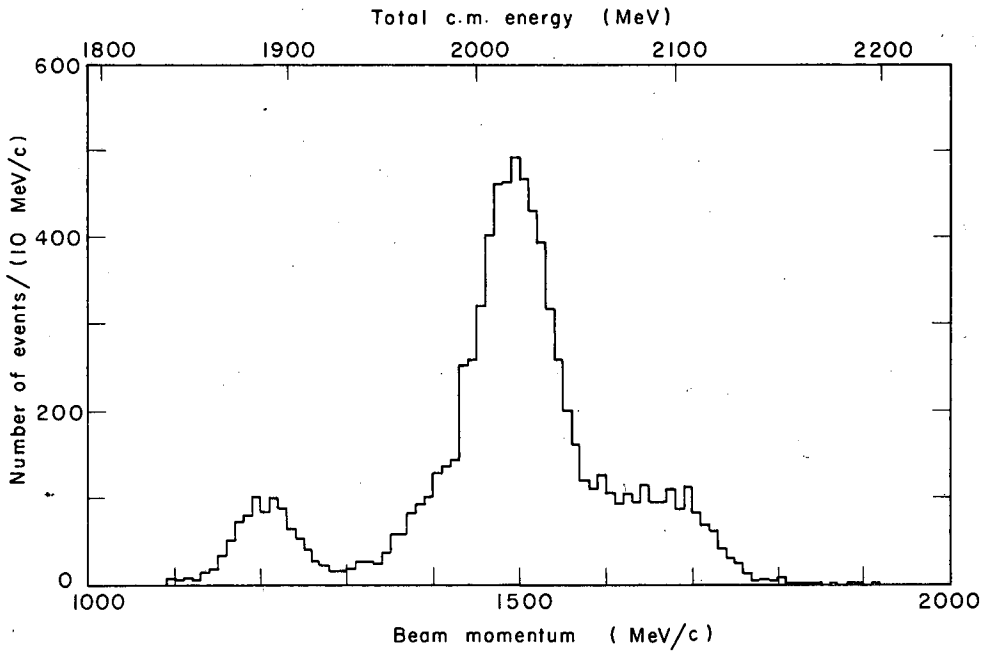

Fig. 2. Unfitted beam-track momentum spectrum of 8408 events in which $\bar{K}^0$'s are produced.

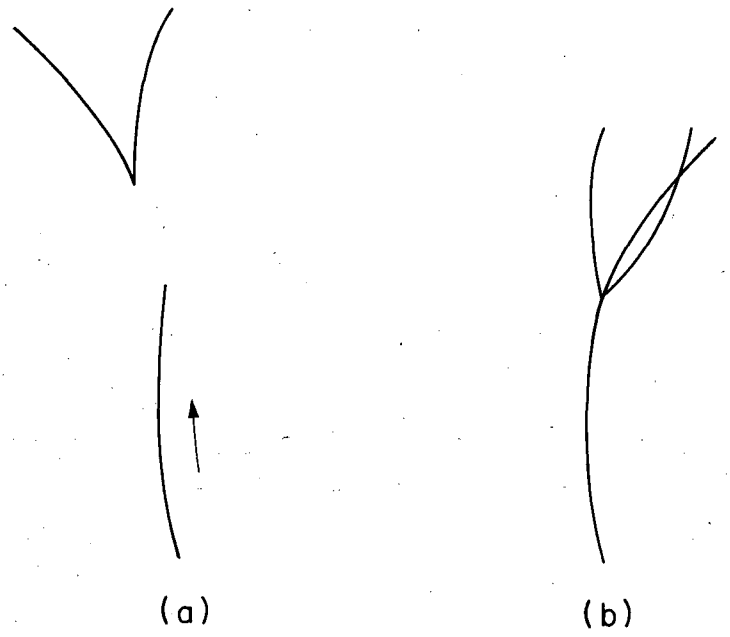

Fig. 3. Bubble-chamber topologies. (a) Charge-exchange scatter with subsequent $K_1^0 \rightarrow \pi^+ + \pi^-$ decay of the $\overline{K}^0$; (b) K^- decay into three charged particles.

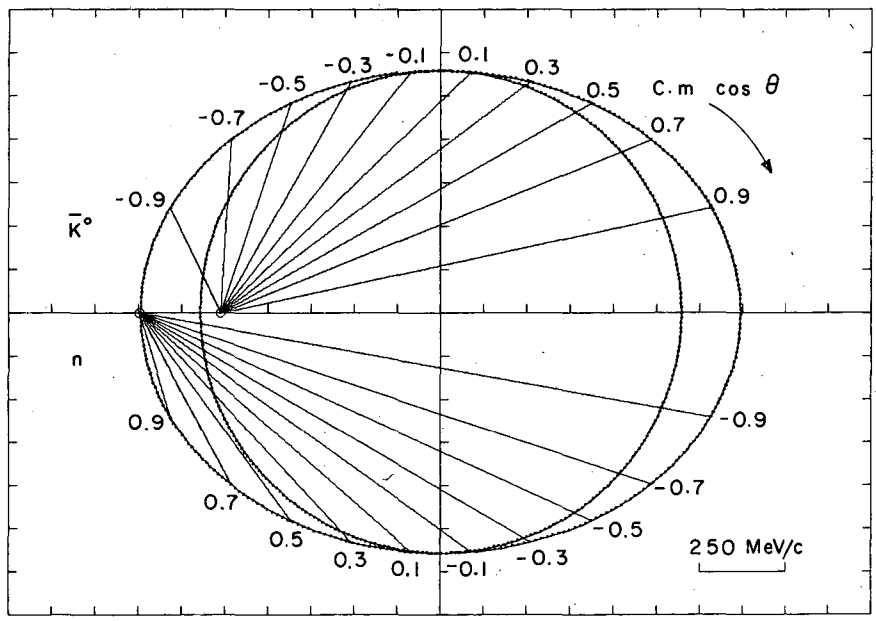

Fig. 4. An ellipse plot, displaying the kinematics of the reaction $K^- + p \rightarrow \bar{K}^0 + n$ when the K^- laboratory momentum is 1.51 BeV/c. The radius of the circle equals the (final-state) c. m. momentum. Laboratory momenta and angles corresponding to various c. m. production $\cos\theta$ can be read off directly; $\bar{K}^0$ quantities are in the upper half, n quantities are in the lower.

and consequently had least statistical significance; the discrepancies between the two scans in about 2/3 of the film at each of these momenta were resolved. All of the discrepancies at 1.70 BeV/c were resolved.

Had all of the 1.51-BeV/c film been used to determine the charge-exchange cross section, the statistical error (2-1/2%) would have been smaller than systematic uncertainties. Consequently, while all of this film was used to establish the angular distribution, the normalization was obtained from only about 30% of it, and only in this portion were scans compared and resolved.

Finally, about 4×10^4 pictures scattered throughout the film (20% of the film in which scans were compared) were subjected to a careful third scan. Scanning losses were corrected separately at each momentum, since the scanners grew more proficient with time. If one assumes that three scans disclosed all of the events, single-scan efficiencies were between 90 and 96%, while double-scan efficiencies were between 97 and 99%. The efficiencies for V 0-prongs and 3-prongs were usually quite similar. No significant correlations of kinematics with scanning efficiency were noted.

C. Measuring

The V 0-prong events were measured on a Franckenstein, a very accurate and reliable measuring device. Essentially it is a projection microscope that can measure and record the coordinates of points on the film. The film is mounted on a stage that controls its movement across the optical centerline of the microscope. The measurer sets a track on a cross hair. The film is set in motion and an optical feedback mechanism keeps the track on the cross hair. The x-y coordinates of a number of points on each track of the event, in each of three views, are recorded. The coordinates of fiducial marks on the bubble-chamber window are measured in order to provide a frame of reference for the event. All this information, as well as indicative scan data, are put on tape, which then is processed by computer.

Events that failed to fit any hypothesis (see Sec. III) were remeasured as many as three times. Finally all remaining events except those in the portion of film at 1.51 BeV/c not used to determine the total charge-exchange cross section were re-examined on the scan table. This was done by one person so that the treatment would be uniform and accurate. The correction for unmeasurable and otherwise unpassing events was 2-1/2 to 4-1/2%, varying somewhat with momentum. With few exceptions all events were accounted for. No significant correlations of kinematics with unpassing events were noted.

D. Computer Analysis

The measurements were processed with the standard Alvarez Group data-reduction programs PANAL, PACKAGE, EXAMIN, LINGO, READX, SUMX, and DJINN.[3] PANAL performs simple checks on and reorders the measured data. PACKAGE consists of two parts. The first, PANG, uses the digitized points to reconstruct each of the tracks in space; it assigns to each of them one or more mass hypotheses, depending on the event type, and computes momenta and space angles and their errors. The second part, KICK, performs least-squares fits for possible interpretations of the event, using the equations of momentum and energy conservation at the vertices as constraints. Fitted quantities are computed for the tracks of passing events. EXAMIN uses these quantities to compute information of particular interest to the physicist, such as center-of-mass production angles, polarizations, and invariant masses of various combinations of particles. LINGO is a merging and bookkeeping program; EXAMIN output tapes are merged onto a data summary tape, while a record of the progress of each event is kept on the master list. The master list is used to produce tallies, lists, etc. READX edits the data-summary tape, imposing various selection criteria, and, if necessary, calculates additional quantities of interest. The edited tape is input to SUMX, which produces histograms, scatter-plots, etc. for various subsets of events, thus summarizing and displaying relevant physics information. DJINN performs least-squares fits to angular distributions.

III. ANALYSIS OF THE DATA

A. Kinematic Fitting

At these momenta, the V 0-prong topology can exemplify any of the following reactions:

$$\left.\begin{array}{l} K^- + p \rightarrow \overline{K}^0 + n \\ \quad\quad \rightarrow \overline{K}^0 + n + \pi^0\text{('s)} \end{array}\right\} \quad \overline{K}^0\,(K_1^0) \rightarrow \pi^+ + \pi^- \qquad (1)$$

$$\left.\begin{array}{l} K^- + p \rightarrow \Lambda + \pi^0 \\ \quad\quad \rightarrow \Lambda + \pi^0 + \pi^0\text{ ('s)} \\ \quad\quad \rightarrow \Sigma^0 + \pi^0 \\ \quad\quad \rightarrow \Sigma^0 + \pi^0 + \pi^0\text{ ('s)} \end{array}\right\} \Sigma^0 \rightarrow \Lambda + \gamma \Bigg\} \Lambda \rightarrow p + \pi^-$$

Other reactions that "contaminate" the topology are discussed in Sec. III. G.

The kinematic fitting was done one vertex at a time. The constraints were the four equations of energy and momentum conservation. In a fit to a given hypothesis, the assignment of the appropriate mass to a track relates its energy to its measured momentum. Then the number of constraints at the vertex (and the mean value of the theoretical χ^2 distribution for that number of constraints) is (4 - N), where N is the number of track momentum components that are not determined by the measurement. Values of χ^2's less than ten times the number of constraints were considered acceptable. The fitting procedure was:

(a) Decay vertex. For each of the possibilities, K_1^0 and Λ, two fits were attempted. (i) The information on the direction of the decaying neutral from the 0-prong was used. The only missing piece of information was the magnitude of the neutral momentum. Therefore there were three constraints. (ii) The information on the direction of the neutral was disregarded; the number of constraints was reduced to one. In addition, the neutral (extended backward) had to cross within 8 mm beyond the last bubble of the beam track. This allowed a few events with obscured beam tracks or slight scatters of the decaying neutral to pass. (About 97% of the final set of good events passed at least the three-constraint hypothesis.)

(b) Production vertex. Data on the decaying neutral were transferred to the production vertex. Only the first and third of the listed reactions are constrained. An event either had to fit one of these one-constraint hypotheses, or the invariant mass of the system of undetected neutrals had to be above the minimum for an appropriate unconstrained channel.

About 15% of the events that fit the charge-exchange reaction also fit some Λ hypothesis. The problem of resolving these ambiguous events is taken up in Sec. III. D.

B. Fiducial Criteria

Events with vertices near the edges of the chamber, where the illumination and (or) other factors affecting film and track quality are poor, suffer from three deficiencies: (a) the scanning efficiency is not as high as in the center of the chamber; (b) the tracks are frequently not long enough for accurate measurement; (c) the likelihood is appreciable that even short-lived particles will decay outside the chamber. For these reasons, events were rejected if their production and decay vertices did not fall within inner and outer fiducial volumes, respectively. The distance between the "walls" of the inner and outer fiducial volumes was 7 cm at the downstream end of the chamber and 2 cm elsewhere. A K_1^0 produced in the inner region was quite unlikely to decay beyond the confines of the outer walls. Corrections were made for the few escaping events (see Sec. III. C). A track leaving the outer volume was measureable for about 10 cm if at the front or rear of the chamber, and for at least 1 cm if elsewhere.

C. Length of the Decaying Neutral

Events with only a small gap between production and decay vertices were quite likely to be lost among the numerous 2-prong events. Since the latter were not scanned or measured, there was no way to recover the real V 0-prongs from among them. The loss was especially large for $\overline{K}^0$'s produced in backward directions, since these have quite low momenta in the lab. system. The kinematics are displayed in Fig. 4.

Events with a gap less than 5 mm between vertices were rejected. For each event passing the fiducial-volume and minimum-length criteria, the probability was calculated that the neutral would decay in the interval (along the line of flight) between 5 mm and the wall of the outer volume. The inverse of this "detection probability" was the weight for the event. With w_i the weight for the ith event, the corrected total number of events and error is

$$N \pm \delta N = \Sigma_i w_i \pm (\Sigma_i w_i^2)^{1/2}. \qquad (2)$$

The overall correction for K_1^0 decays falling outside the fiducial volume was only about 1%. The correction for events with short gaps was considerably larger. Figure 5 is a graph of the latter weight versus the center-of-mass (c.m.) production angle for the events at 1.51 BeV/c.

The above calculations were done using several different cutoff lengths in order to insure that 5 mm was indeed large enough so that events with greater lengths would be found with close to 100% efficiency. For the data at 1.51 BeV/c, Fig. 6 shows as a function of cutoff length (a) the weighted total number of events, and (b) the weighted number in the backwardmost production angle bin, which is most sensitive to the effect.

After the above criteria were imposed, there remained 8408 events (before weighting) that fit a K_1^0 hypothesis unambiguously (i.e., fit no Λ hypothesis). Figure 7 shows the spectrum of the square of the invariant mass of the system of undetected neutrals recoiling against the K_1^0. Separation between the neutron peak and events with π^0's is almost complete; mixing between them is less than 1%. As the momentum increases, the many-body final states become more important; from low to high momentum, the fractions in the neutron peak are 69, 50, 48, 48, and 42%, respectively. Some enhancement appears in the vicinity of the $N^*_{3/2}(1238)$.

D. Ambiguous Events

In the following discussion the data at 1.51 BeV/c are used as an example. The data were treated in the same way at all momenta.

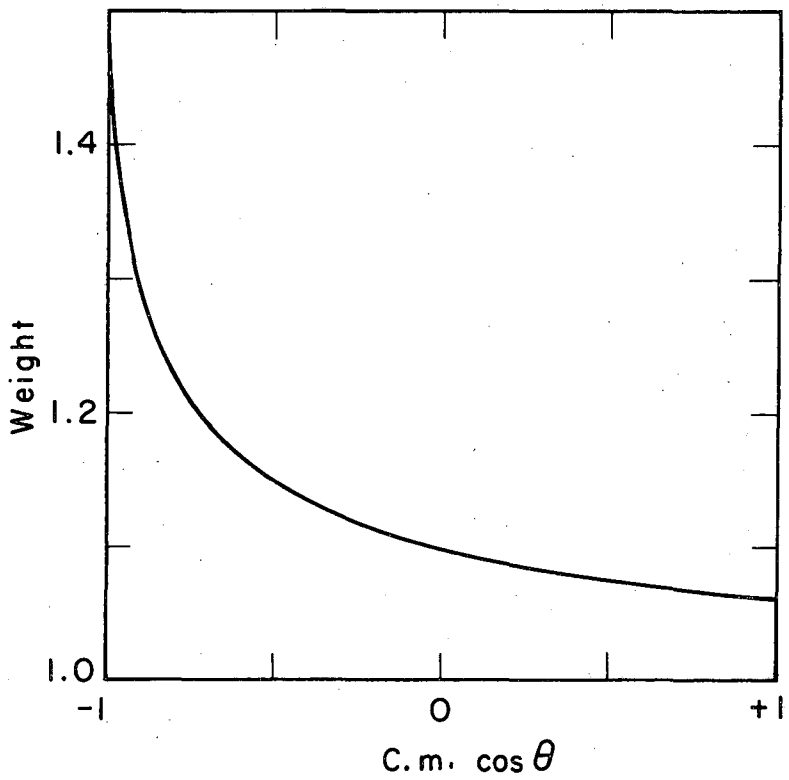

MU-36282

Fig. 5. The weight factor, as a function of c.m. production $\cos\theta$, when the K^- laboratory momentum is 1.51 BeV/c, to be applied to charge-exchange events with a gap between vertices greater than 0.5 cm in order to correct for those events with a shorter gap; given by $\exp(L_0 m/pc\tau_0)$, where L_0 = 0.5 cm, m = 498 MeV, $c\tau_0$ = 2.76 cm,[5] and p is the K_1^0 laboratory momentum in MeV/c. The last quantity can be obtained from Fig. 4.

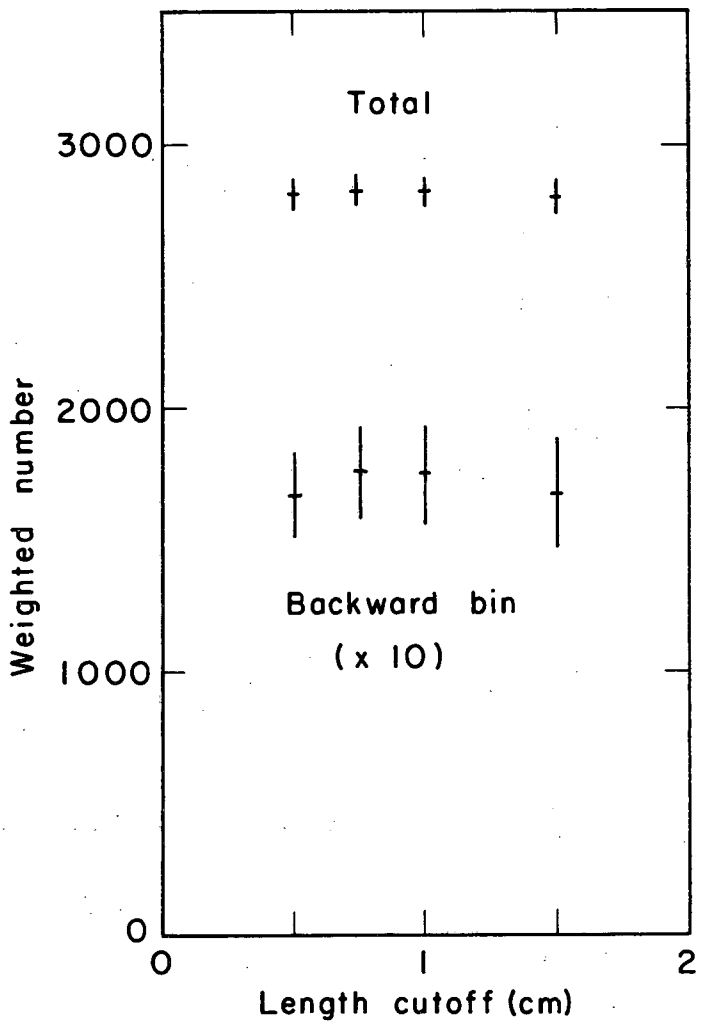

Fig. 6. For the data at 1.51 BeV/c, as a function of gap cutoff length, (a) the total weighted number of events, and (b) the weighted number in the backwardmost production angle bin. Since the K_1^0 laboratory momenta are lowest there, this bin is most sensitive to the cutoff length. The data show that 0.5 cm is a sufficient cutoff length.

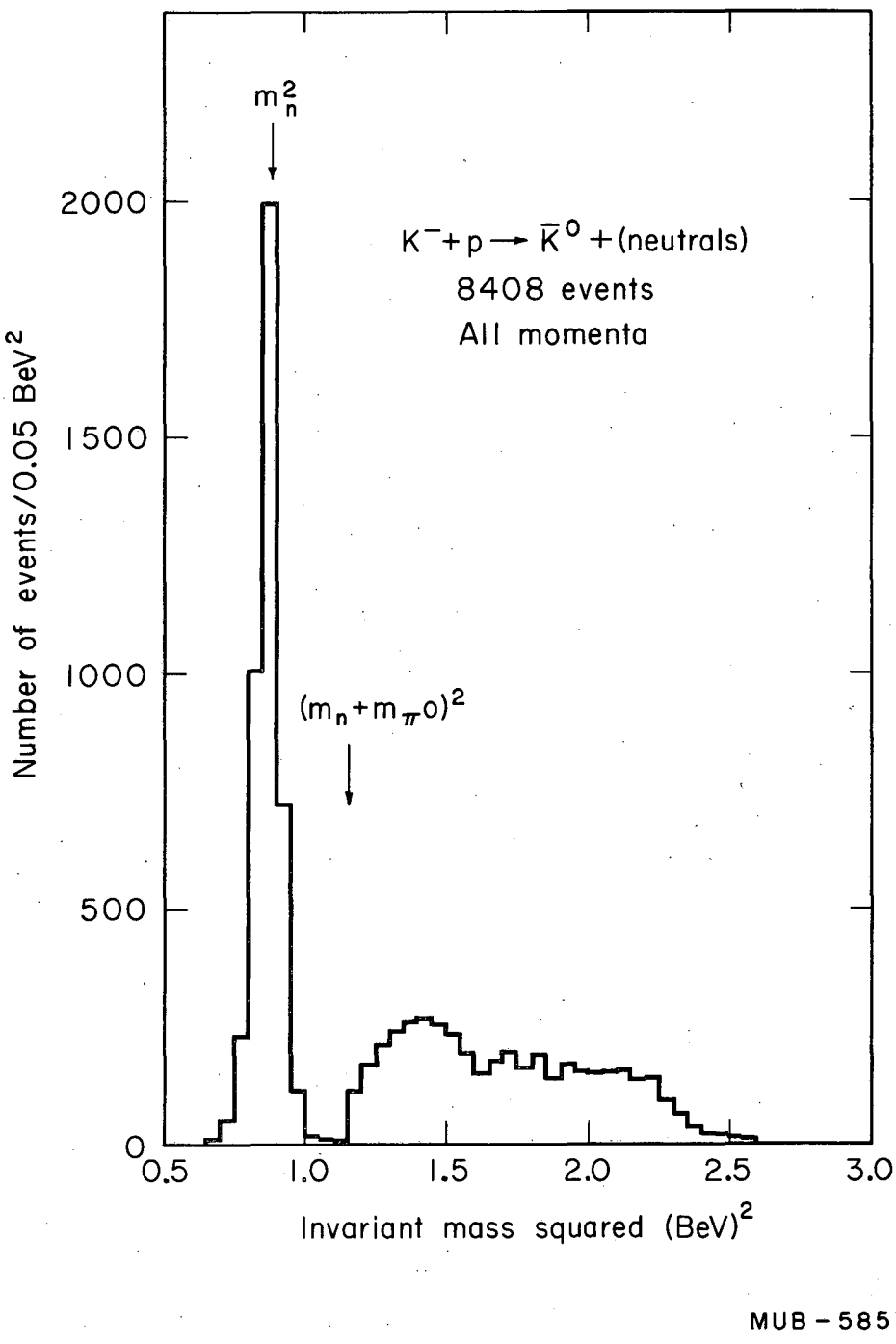

Fig. 7. Square of the invariant mass of the system of undetected neutrals recoiling against the K_1^0 (all momenta).

At 1.51 BeV/c, 2798 events fit the reaction $K^- + p \rightarrow \overline{K}^0 + n$ and satisfied the "geometrical" requirements of the previous two subsections. Of these events, 414 also fit some Λ hypothesis. While many of the ambiguities could be resolved by looking at the ionization of the positive decay particle, often it was impossible to do so. Either the track momentum was too high for the ionization to be very different for a proton or π^+, or the track was too steep with respect to camera directions for the ionization to be apparent, or some other difficulty prevailed.

Another solution to the problem was available. Figure 8 is a scatter-plot of the ambiguous events. For purposes of the plot, they are considered to be K_1^0's. The abscissa is the production-angle cosine in the K^-p c.m. system. The ordinate is the cosine of the angle between the π^+ and K_1^0 directions, in the decay rest frame. Of the 414 events, 397 fall within the region bounded by (a) a production-angle cosine greater than -0.2 and (b) a decay-angle cosine greater than +0.7. All events falling within these limits, whether ambiguous or unambiguous, were excluded from further analysis. Since the K_1^0 decay distribution should be isotropic, the accepted events with production-angle cosine greater than -0.2 were weighted with a factor 20/17. Figure 9 shows that the decay distribution outside the region of ambiguity is indeed isotropic.

Why only a small part of the kinematic region open to K_1^0 events is open to Λ events is readily understood:

(a) At 1.51 BeV/c the maximum laboratory angle for Λ production is 59 deg. Charge-exchange scattering produces $\overline{K}^0$'s at all laboratory angles; 59 deg corresponds to a c.m. production-angle cosine of -0.2. See Fig. 4.

(b) In the decay frame, the momentum of the particles produced in the process $\Lambda \rightarrow p + \pi^-$ is 100 MeV/c. The corresponding momentum for the decay $K_1^0 \rightarrow \pi^+ + \pi^-$ is 206 MeV/c. An event in which the positive decay particle has a laboratory momentum component transverse to the line of flight of the decaying neutral greater than 100 MeV/c must be a K_1^0; the Lorentz transformation from the laboratory frame to the decay

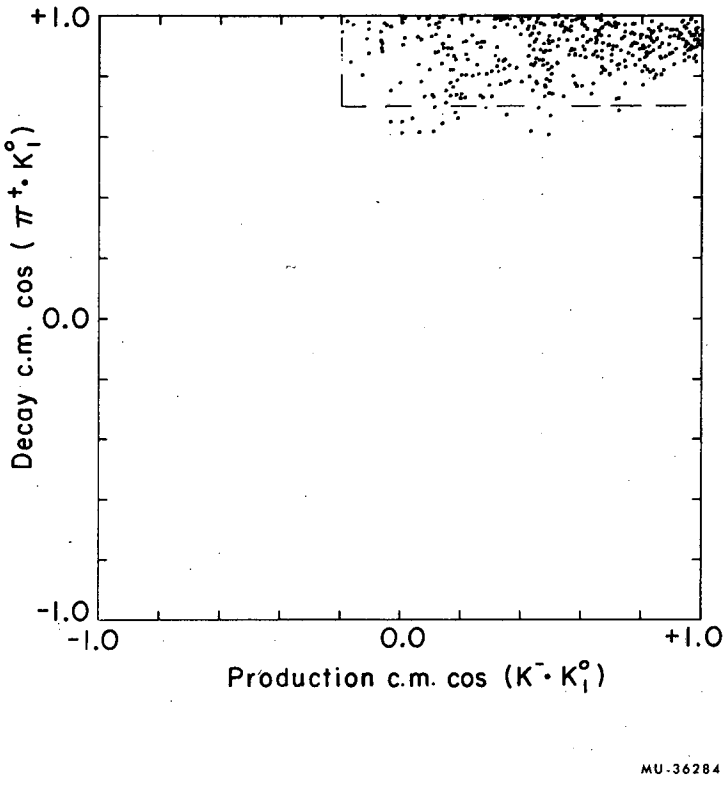

Fig. 8. Ambiguous events at 1.51 BeV/c, treated here as K_1^0's.

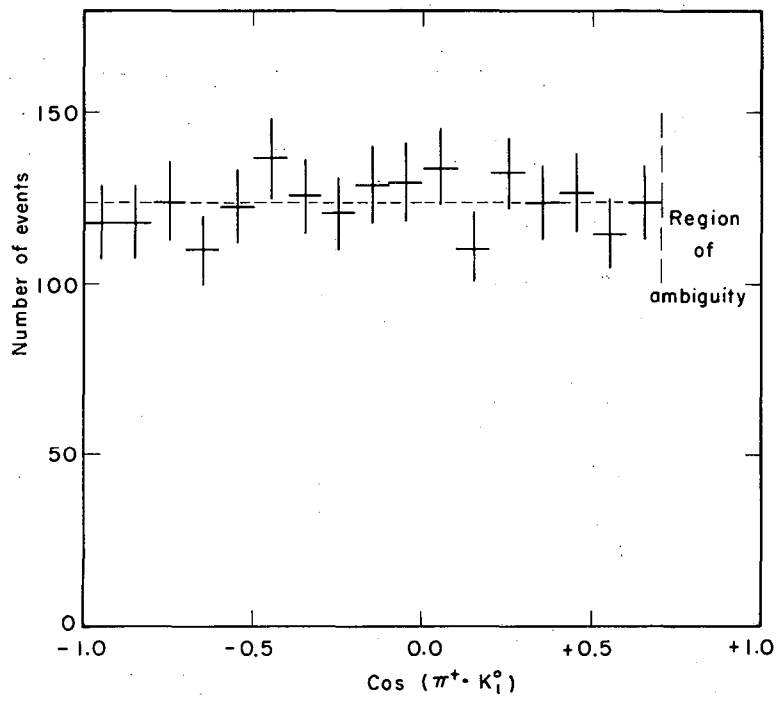

Fig. 9. Distribution $\cos(\pi^+ \cdot K_1^0)$ in the K_1^0 rest frame for the accepted charge-exchange events at 1.51 BeV/c.

frame does not alter the transverse momentum. Viewed in the rest frame of K_1^0 decay, a transverse momentum of 100 MeV/c corresponds to decay-angle cosines between π^+ and K_1^0 directions equal to ±0.87. Two cones are cut out of the sphere representing possible K_1^0 decay directions. Furthermore, only the forward cone, defined by the limit +0.87, is open to Λ events. The Λ's that are possible according to requirements of production kinematics have too much momentum in the laboratory to simulate K_1^0's having the π^+ in the backward cone. The small energy release of Λ decay requires the proton momentum to be largely along the Λ line of flight. Conversely, only those K_1^0 events with the π^+ in the forward cone can simulate Λ's that are fast enough in the laboratory system to satisfy production kinematics.

In practice, the limit +0.87 is weakened. The transverse momentum component cannot always be accurately determined by the measurement; thus it can be "pulled" when the event is fitted. See Fig. 8.

Since Λ events are restricted to a small part of the kinematic range open to K_1^0 events, more Λ events can simulate K_1^0 events than vice versa. In excluding the region into which the ambiguous events fell, 207 events were discarded that fit only the charge-exchange reaction. According to the decay distribution outside the barred region, 277 K_1^0 events were present within the region. Therefore 70, or 18%, of the 397 ambiguous events were K_1^0 events.

In summary, at 1.51 BeV/c, a total of (2798-414-207) = 2177 events passed all acceptance criteria. Correction for fiducial volume, minimum neutral length, and ambiguous region cutoffs brought the number up to 2809 ±61. See Table I.

E. Neutral and Long-Lived $\overline{K}^0$ Decay Modes

Half of all $\overline{K}^0$'s decay by long-lived, 3-body K_2^0 modes. Few of these were seen at all; those that were, were rejected by the fitting procedure. The branching fraction for the decay mode $K_1^0 \rightarrow \pi^+ + \pi^-$ is 69.4 ±1.1%.[5] Thus the correction factor for neutral and long-lived decay modes of the $\overline{K}^0$ is 2.88 ±0.05. The error in this quantity has not been folded into the results because it does not affect the relative behavior of the cross sections at the various momenta.

Table I. Charge-exchange cross sections, with numbers of events, correction factors, and path-length values.

Momentum (MeV/c)	Events[a]	Weighted events[b]		Scan and measure loss (%)	Events/mb		σ mb
		Number	Error (%)		Number	Error (%)	
1220	573	752	4.2	6.5	816	2.6	2.83 ±0.14
1420	342	440	5.4	7.5	718	3.0	1.90 ±0.12
1510 select[c]	547	704	4.3	5.7	1169	2.4	1.83 ±0.09
1510 total[d]	2177	2809	—	—	—	—	—
1600	304	392	5.8	6.0	619	3.4	1.93 ±0.13
1700	408	528	5.0	4.5	956	2.8	1.66 ±0.10

[a] After all cutoffs and before any corrections.

[b] Corrected for cutoffs in fiducial volume, length of neutral, and region of ambiguity.

[c] Cross section obtained from this sample.

[d] Differential cross section obtained from all events.

F. Normalization

The K^- path length was determined by counting 3-prong events (Fig. 3). Most of these were τ decays, $K^- \rightarrow \pi^+ + \pi^- + \pi^-$. Some, however, resulted from K^- decay modes in which a Dalitz $e^\pm$ pair could be produced. The rate of decay by this latter process is 7% of that of τ decay.[5] The 3-prongs were not measured, and the Dalitz events could not be completely separated from τ events on the scanning table. Since all are unambiguous signatures of K^- decay, all were included in the scan.

Of interest is the number of 3-prongs within the inner fiducial volume. The scan information for each event included a zone number giving its location in the bubble chamber. The systematic error inherent in counting events according to zone number rather than accurately measured locations was not above 1%.

The path lengths, in events/mb, are included in Table I. Corrections for scan losses have been made. The branching fraction for K^- decay into 3-prongs is $(5.88 \pm 0.17)\%$.[5] The 3% uncertainty in this number was not folded into cross-section determinations, because relative values are not affected.

G. Other Systematic Effects; Systematics and Statistics

In the whole experiment there were about 100 events in which a Ξ^0 was produced and the Λ and K_1^0 decays were visible[4] ($K^- + p \rightarrow \Xi^0 + K^0$, $\Xi^0 \rightarrow \Lambda + \pi^0$). Therefore, there are about 50 such events with only the K_1^0 decay visible. These, however, cannot contaminate the charge-exchange channel, since the Ξ^0 mass is well above the neutron mass; the events fall in the continuum of the mass spectrum of Fig. 7.

The charge-exchange reaction involves no π^0's or γ rays at either vertex; consequently there can be no $e^\pm$ pairs present to alter the topology.

The number of events in which the $\overline{K}^0$ interacted before it would have decayed by the K_1^0 mode was less than 1%.[6] Similarly, the number

of events in which one of the π's from the K_1^0 decay had a track less than 1 cm in length was less than 1%. Other small biasing effects were equally negligible.

The effects of biases have been corrected with considerable accuracy. If the uncertainties of K^- and K_1^0 branching ratios are neglected, the overall systematic errors of cross-section determinations are probably smaller than the statistical errors of 5 to 7%. Because the data at the various momenta have been treated in the same way, the relative systematics should be even smaller. The errors quoted in Sec. IV are statistical only.

IV. RESULTS OF THE ANALYSIS

A. Cross Sections

The charge-exchange cross sections are given in Table I, and appear in Fig. 10 with results of other experiments between 0.3 and 3.0 BeV/c.[7-17] Some of the experimental results have been changed slightly where different values of K^- and K_1^0 branching fractions have been used. The cross section in the vicinity of 1.0 BeV/c is dominated by the $Y_1^*(1765)$ and the $Y_0^*(1815)$ resonant states. Above this region the cross section decreases slowly with increasing momentum, with little significant evidence of structure.

B. Angular Distributions

The differential cross sections are given in Table II and are displayed in Figs. 11 through 15. At 1.51 BeV/c, where there are many events, the data are split into 40 bins. At the other momenta, there are 21 bins--a basic 20, but with either the backward bin (at 1.22 or 1.42 BeV/c) or the forward bin (at 1.60 and 1.70 BeV/c) split in two.

Each of the distributions has been fit with a Legendre polynomial series,

$$\frac{d\sigma}{d\Omega} = \frac{\lambda^2}{4} \sum_{n=0}^{n_{max}} B_n P_n(\cos\theta), \tag{3}$$

by using the method of least squares. Here $\lambda = \hbar/q$ is the reduced wave-length in the K^-p c.m. system (q is the c.m. momentum), θ is the c.m. scattering angle, the $P_n(\cos\theta)$ are the Legendre polynomials, the best value of n_{max} and of the coefficients B_n are to be determined by the fit, and the factor 4 arises from the isotopic spin decomposition of the scattering amplitude

$$A(K^- + p \rightarrow \overline{K}^0 + n) = \frac{A(I = 1) - A(I = 0)}{2} . \tag{4}$$

The angular distribution is equal to the square of the amplitude; $A(I = 0)$ and $A(I = 1)$ are the elastic scattering amplitudes in the pure isotopic spin states.

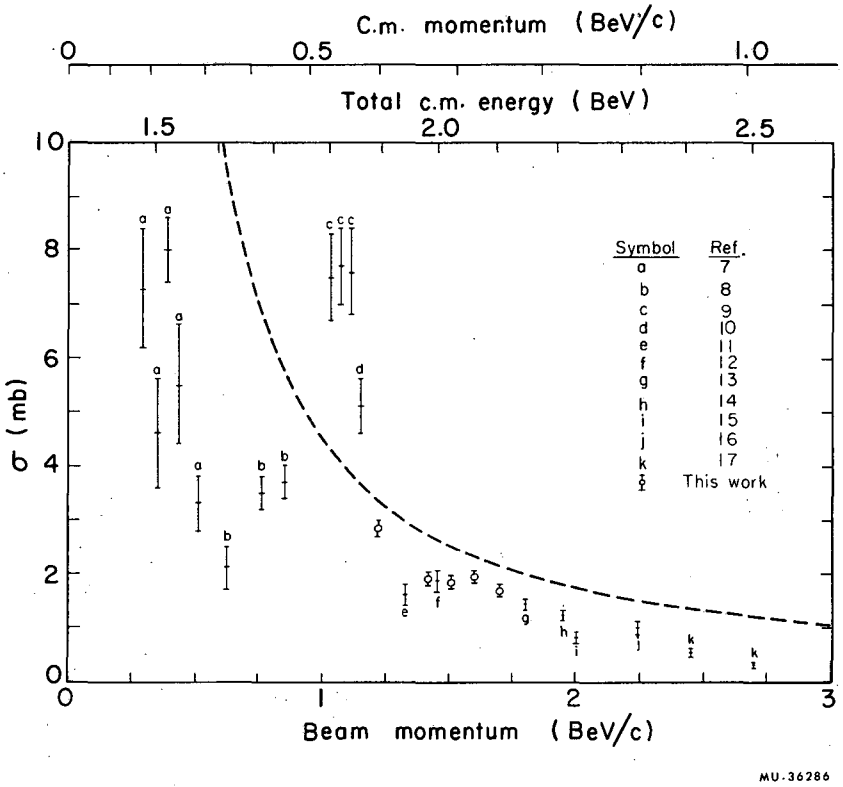

Fig. 10. The K^-p charge-exchange cross section as a function of beam momentum, total c.m. energy, and c.m. momentum. The dashed curve is $\pi\lambda^2$.

Table II. Differential charge-exchange cross sections in mb/sr. The errors are based on the statistics of the angular distributions alone. The normalization errors, which affect all points at a given momentum in the same way, are not included.

Cos	Momentum (MeV/c)				
	1220	1420	1510	1600	1700
-1.0	1.270± 0.150	0.367± 0.085	0.346± 0. 032	0.225± 0.050	0.079± 0.024
-0.9	0.534± 0.095	0.372± 0.084	0.172± 0. 022		
-0.9	0.252± 0.045	0.196± 0.042	0.094± 0. 016	0.060± 0.024	0.038± 0.016
-0.8			0.047± 0. 011		
-0.8	0.151± 0.034	0.043± 0.019	0.046± 0. 011	0.048± 0.021	0.073± 0.021
-0.7			0.068± 0.013		
-0.7	0.111± 0.029	0.132± 0.033	0.072± 0.013	0.065± 0.025	0.065± 0.020
-0.6			0.100± 0.016		
-0.6	0.152± 0.033	0.141± 0.034	0.069± 0.013	0.202± 0.043	0.089± 0.023
-0.5			0.092± 0.015		
-0.5	0.229± 0.040	0.130± 0.032	0.108± 0.016	0.100± 0.030	0.064± 0.019
-0.4			0.107± 0.016		
-0.4	0.269± 0.044	0.121± 0.031	0.079± 0.014	0.037± 0.019	0.046± 0.016
-0.3			0.081± 0.014		
-0.3	0.230± 0.040	0.072± 0.024	0.053± 0.011	0.097± 0.029	0.029± 0.013
-0.2			0.060± 0.012		
-0.2	0.115± 0.031	0.065± 0.025	0.048± 0.012	0.094± 0.032	0.088± 0.024
-0.1			0.055± 0.013		
-0.1	0.121± 0.031	0.018± 0.013	0.067± 0.014	0.119± 0.036	0.046± 0.017
0.0			0.041± 0.011		
0.0	0.056± 0.021	0.065± 0.024	0.100± 0.017	0.094± 0.032	0.139± 0.031
0.1			0.099± 0.017		
0.1	0.041± 0.018	0.100± 0.030	0.093± 0.016	0.136± 0.038	0.156± 0.032
0.2			0.118± 0.018		
0.2	0.095± 0.027	0.163± 0.038	0.131± 0.019	0.151± 0.041	0.122± 0.029
0.3			0.187± 0.023		
0.3	0.113± 0.030	0.153± 0.037	0.223± 0.025	0.246± 0.050	0.143± 0.031
0.4			0.166± 0.021		
0.4	0.192± 0.039	0.197± 0.042	0.183± 0.023	0.135± 0.038	0.086± 0.024
0.5			0.175± 0.022		
0.5	0.300± 0.049	0.205± 0.043	0.172± 0.022	0.127± 0.037	0.071± 0. 021
0.6			0.166± 0.021		
0.6	0.271± 0.046	0.222± 0.044	0.184± 0.022	0.110± 0.033	0.116± 0.027
0.7			0.172± 0.022		
0.7	0.323± 0.050	0.115± 0.032	0.217± 0.024	0.216± 0.048	0.272± 0.043
0.8			0.273± 0.027		
0.8	0.301± 0.048	0.309± 0.053	0.276± 0.027	0.388± 0.062	0.391± 0.050
0.9			0.305± 0.029		
0.9	0.272± 0.046	0.209± 0.043	0.399± 0.033	0.414± 0.090	0.555± 0.085
1.0			0.378± 0.032	0.429± 0.094	0.495± 0.080

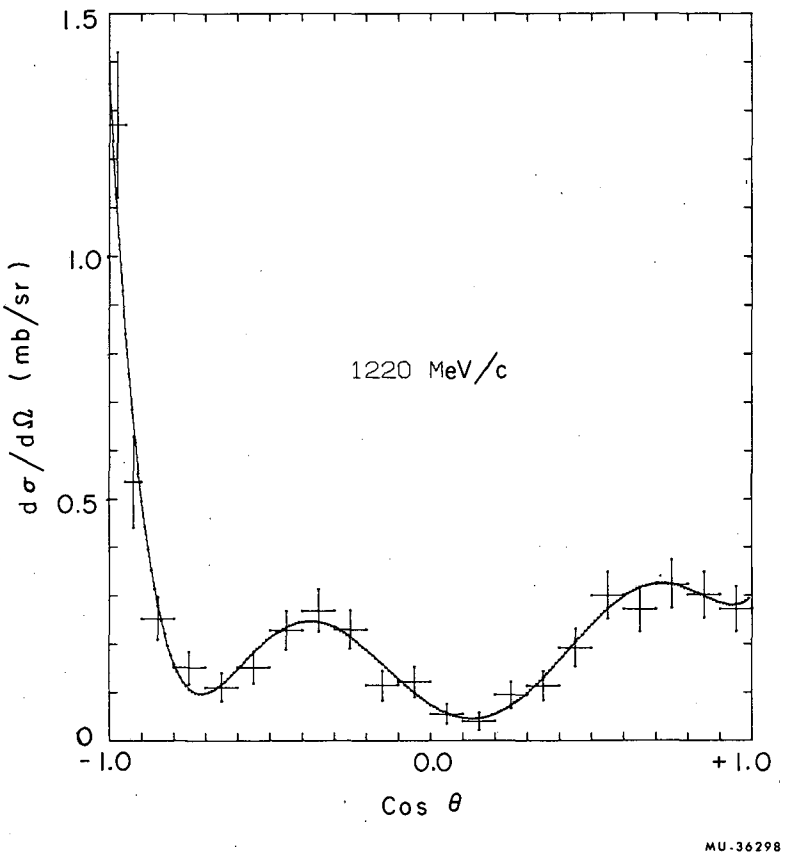

Fig. 11. Differential cross section for charge-exchange scattering at 1.22 BeV/c. The curve is taken from the fit with $n_{max} = 6$.

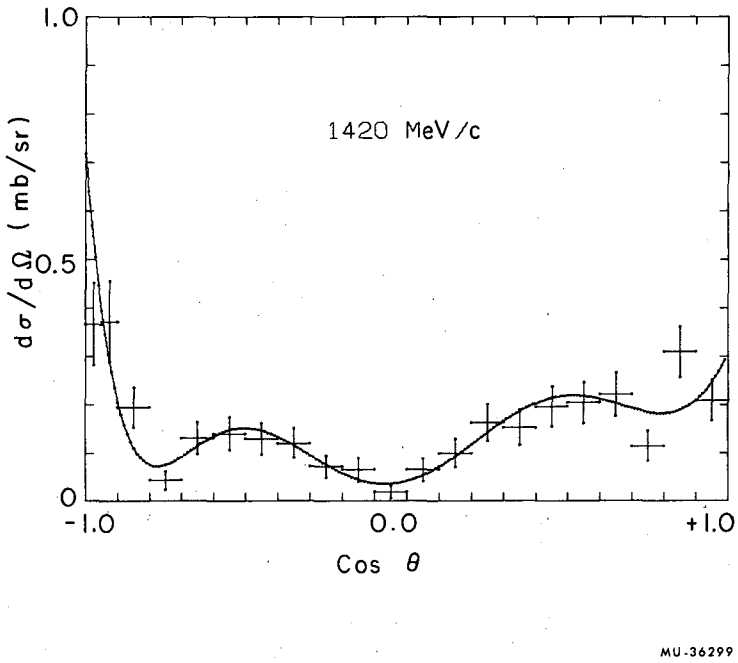

Fig. 12. Differential cross section for charge-exchange scattering at 1.42 BeV/c. The curve is taken from the fit with $n_{max} = 7$.

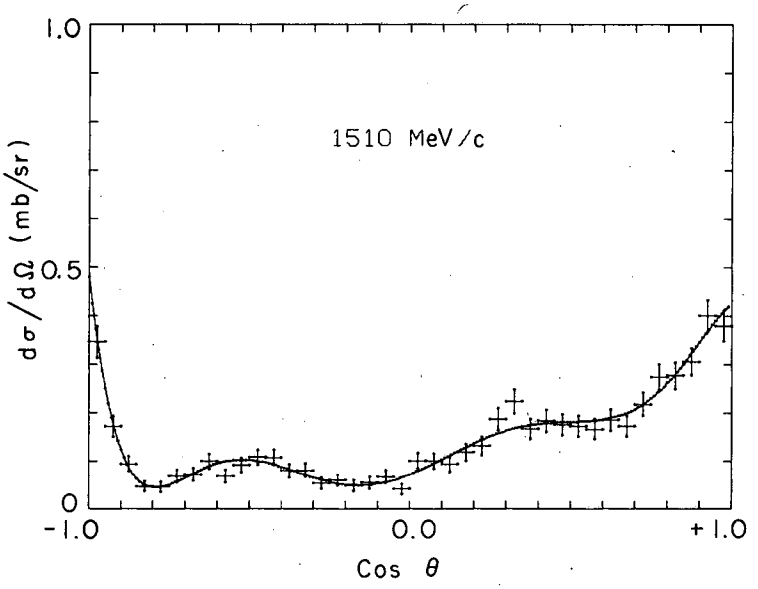

Fig. 13. Differential cross section for charge-exchange scattering at 1.51 BeV/c. The curve is taken from the fit with $n_{max} = 7$.

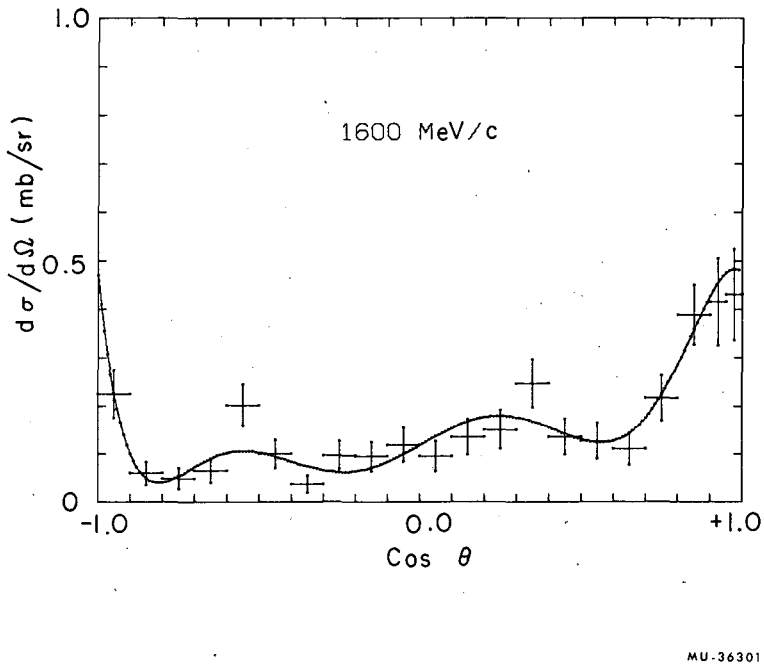

Fig. 14. Differential cross section for charge-exchange scattering at 1.60 BeV/c. The curve is taken from the fit with $n_{max} = 7$.

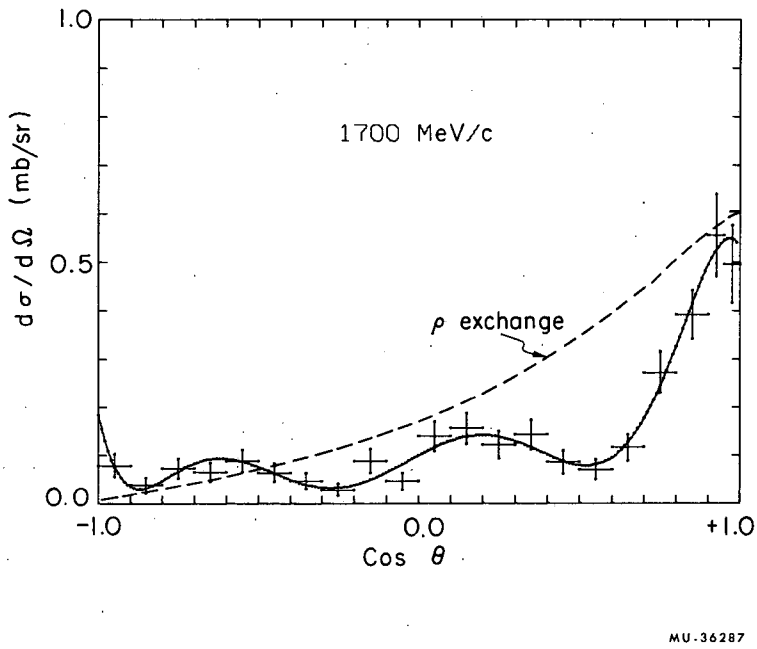

Fig. 15. Differential cross section for charge-exchange scattering at 1.70 BeV/c. The solid curve is taken from the fit with $n_{max} = 7$. The dashed curve is the prediction of the simple ρ-exchange model; this curve is arbitrarily normalized at 0.6 mb/sr in the forward direction.

Fits were obtained for values of n_{max} from 0 to 10. The number of degrees of freedom of a fit is $\nu = (m - n_{max} - 1)$, where m is the number of data bins. The quantity ν is also the mean value of the theoretical χ^2 distribution for ν degrees of freedom, $f(\chi^2, \nu)$. The "confidence level" that a sufficient value of n_{max} has been reached can be defined as the probability that a χ^2 larger than the experimentally determined value, χ_0^2, would have been obtained. This is just the fraction of the area under the theoretical χ^2 distribution curve that lies beyond χ_0^2:

$$C = \int_{\chi_0^2}^{\infty} f(\chi^2, \nu) d\chi^2. \qquad (5)$$

The confidence levels C as a function of n_{max} for each of the momenta are shown in Fig. 16. At 1.22 BeV/c, the series including $P_6(\cos\theta)$ is necessary and sufficient. At 1.51, 1.60, and 1.70 BeV/c, the series including $P_7(\cos\theta)$ is necessary and sufficient. At 1.42 BeV/c, the distribution appears to require at least $P_8(\cos\theta)$. However, for reasons of continuity, it seems reasonable to suppose $P_7(\cos\theta)$ is sufficient, and to regard the discrepancy as being a statistical fluctuation. The difficulty at 1.42 BeV/c is due principally to the behavior of the angular distribution around $\cos\theta = +0.8$, and, to a lesser extent, to the lack of sharp backward peaking.

The angular distributions were also fit using different numbers of data bins, with no essential change in the conclusions.

The fitted curves are included in Figs. 11 through 15. The primary qualitative feature of the angular distributions, as a function of increasing momentum, is the decline of a sharp backward peak and the rise of a blunt forward peak. The two intermediate bumps in the triple-valleyed curve move slowly backward. At 1.60 and 1.70 BeV/c, the forward peak has flattened out or just turned down in the very forward direction.

The expansion coefficients B_n and the goodness-of-fit parameters, for several values of n_{max} at each of the momenta, are given in

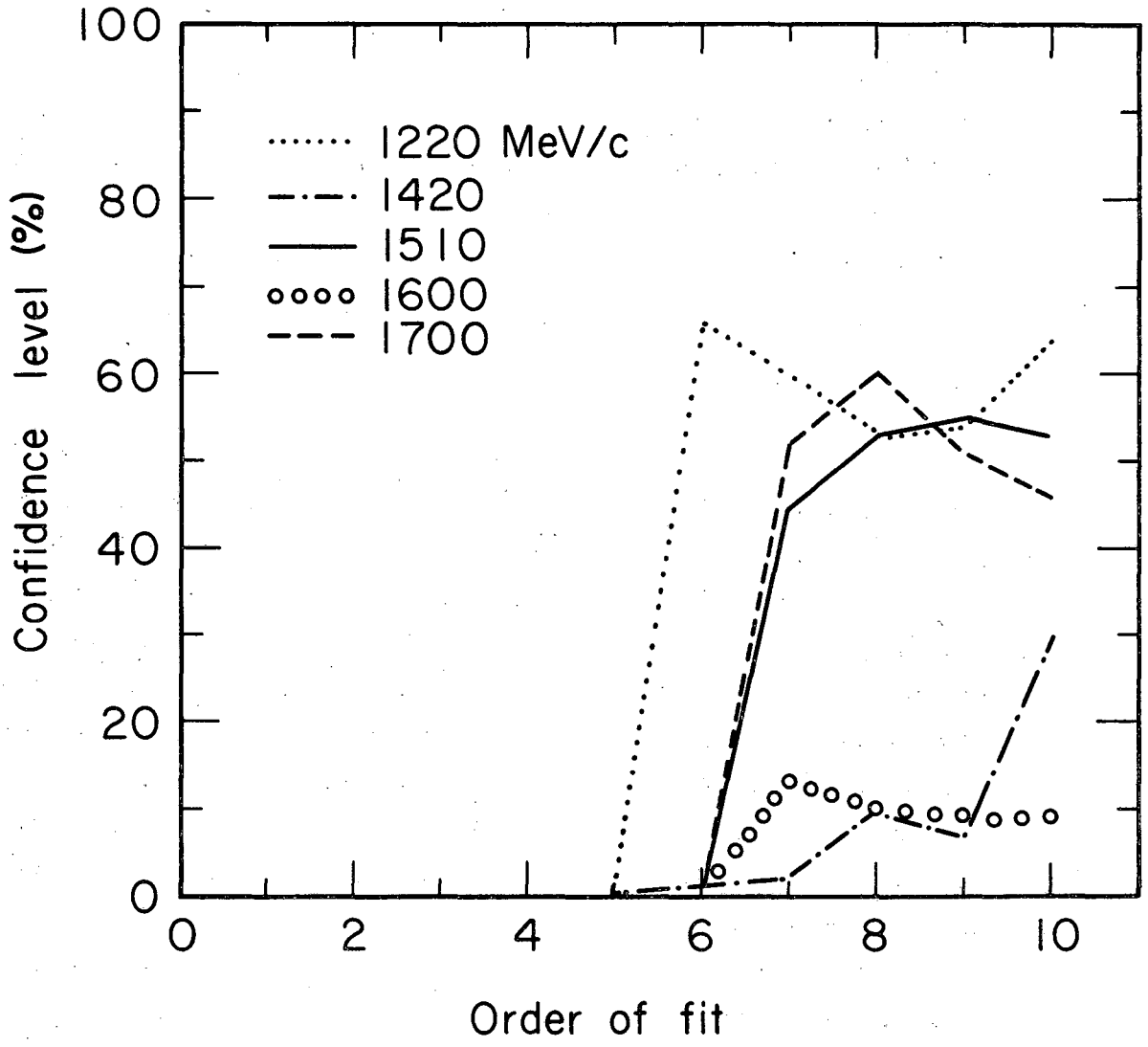

Fig. 16. Confidence levels for the fits to the differential cross sections, as a function of n_{max}.

Table III. The fit obtained by increasing n_{max} by 1 generally changes previously obtained coefficients by little. This is especially true if a good fit has already been obtained, but it remains true to some extent regardless. For example, as noted above, at 1.42 BeV/c the confidence level for $n_{max} = 7$ is low. The fit obtained by increasing n_{max} to 8 raises the confidence level from 1.9% to 10%, but of the coefficients B_0 to B_7, only B_6 is appreciably altered. The "stability" of the coefficients is due to the orthogonality of the Legendre polynomials.[18] Even if the necessary and sufficient value of n_{max} is wrongly chosen, many of the conclusions regarding the behavior of the coefficients remain unchanged. If the angular distributions were expanded in a cosine power series,

$$\frac{d\sigma}{d\Omega} = \frac{\lambda^2}{4} \sum_{n=0}^{n_{max}} A_n \cos^n\theta, \qquad (6)$$

the fitted curves and the confidence levels would be the same as those obtained from the Legendre polynomial expansion. However, an increase of n_{max} would generally cause large changes in those coefficients of powers of $\cos\theta$ having the same "parity" as the new term in the expansion; even (odd) powers of $\cos\theta$ are orthogonal only to odd (even) powers.[19]

Table III. Coefficients, B_n, from the least-squares fits of the differential cross sections to the series $d\sigma/d\Omega = \lambda^2/4 \sum_{n=0}^{n_{max}} B_n P_n(\cos\theta)$.

Momentum (MeV/c)	n_{max}	Expansion coefficients B_0	B_1	B_2	B_3	B_4	B_5	B_6	B_7	B_8	B_9	B_{10}	χ^2	Expected mean χ^2	Confid. level (%)
1220	5	0.79 ± 0.03	-0.07 ± 0.07	0.89 ± 0.09	-0.43 ± 0.11	0.12 ± 0.11	-1.11 ± 0.13						41	15	0
	[6][a]	0.84 ± 0.04	-0.19 ± 0.07	0.98 ± 0.09	-0.57 ± 0.12	0.46 ± 0.13	-1.20 ± 0.13	0.79 ± 0.15					11	14	66
	7	0.84 ± 0.04	-0.19 ± 0.08	0.99 ± 0.10	-0.58 ± 0.12	0.47 ± 0.13	-1.23 ± 0.15	0.79 ± 0.15	-0.06 ± 0.16				11	13	60
	8	0.84 ± 0.04	-0.19 ± 0.08	1.00 ± 0.10	-0.59 ± 0.12	0.47 ± 0.14	-1.23 ± 0.15	0.81 ± 0.17	-0.06 ± 0.16	0.04 ± 0.18			11	12	52
1420	6	0.69 ± 0.04	0.13 ± 0.08	0.59 ± 0.10	-0.45 ± 0.13	0.16 ± 0.13	-0.23 ± 0.14	0.91 ± 0.15					28	14	1.4
	[7]	0.70 ± 0.04	0.11 ± 0.08	0.60 ± 0.10	-0.45 ± 0.13	0.18 ± 0.13	-0.31 ± 0.15	0.87 ± 0.15	-0.30 ± 0.19				26	13	1.9
	8	0.71 ± 0.04	0.12 ± 0.08	0.58 ± 0.10	-0.43 ± 0.13	0.16 ± 0.13	-0.30 ± 0.15	0.60 ± 0.18	-0.39 ± 0.19	-0.55 ± 0.21			19	12	10
	9	0.71 ± 0.04	0.11 ± 0.08	0.58 ± 0.10	-0.42 ± 0.13	0.16 ± 0.13	-0.27 ± 0.16	0.61 ± 0.18	-0.31 ± 0.23	-0.51 ± 0.21	0.14 ± 0.23		18	11	7.4
	10	0.73 ± 0.04	0.11 ± 0.08	0.63 ± 0.10	-0.44 ± 0.13	0.02 ± 0.14	-0.33 ± 0.16	0.40 ± 0.20	-0.43 ± 0.24	-0.94 ± 0.27	-0.06 ± 0.24	-0.62 ± 0.25	12	10	29
1510	6	0.72 ± 0.02	0.53 ± 0.03	0.65 ± 0.04	-0.06 ± 0.05	0.32 ± 0.05	0.03 ± 0.06	0.59 ± 0.06					74	33	0.0
	[7]	0.73 ± 0.02	0.50 ± 0.03	0.68 ± 0.04	-0.11 ± 0.05	0.35 ± 0.06	-0.12 ± 0.06	0.50 ± 0.06	-0.41 ± 0.06				32	32	45
	8	0.73 ± 0.02	0.51 ± 0.03	0.68 ± 0.04	-0.10 ± 0.05	0.34 ± 0.06	-0.11 ± 0.06	0.46 ± 0.07	-0.44 ± 0.07	-0.11 ± 0.07			30	31	53
	9	0.73 ± 0.02	0.51 ± 0.03	0.68 ± 0.04	-0.11 ± 0.05	0.34 ± 0.06	-0.12 ± 0.06	0.47 ± 0.07	-0.47 ± 0.07	-0.13 ± 0.07	-0.09 ± 0.08		28	30	55
	10	0.73 ± 0.02	0.51 ± 0.03	0.68 ± 0.04	-0.12 ± 0.05	0.35 ± 0.06	-0.13 ± 0.06	0.48 ± 0.07	-0.48 ± 0.07	-0.10 ± 0.08	-0.07 ± 0.08	0.07 ± 0.08	28	29	53
1600	6	0.79 ± 0.05	0.64 ± 0.10	0.68 ± 0.14	0.25 ± 0.16	0.70 ± 0.17	0.28 ± 0.18	0.42 ± 0.20					31	14	0.6
	[7]	0.83 ± 0.05	0.60 ± 0.10	0.73 ± 0.14	0.14 ± 0.16	0.71 ± 0.17	0.01 ± 0.19	0.29 ± 0.20	-0.75 ± 0.22				19	13	13
	8	0.83 ± 0.05	0.62 ± 0.10	0.73 ± 0.14	0.14 ± 0.16	0.68 ± 0.18	0.02 ± 0.20	0.25 ± 0.22	-0.79 ± 0.23	-0.13 ± 0.23			19	12	10
	9	0.84 ± 0.05	0.62 ± 0.10	0.74 ± 0.14	0.12 ± 0.16	0.70 ± 0.18	-0.04 ± 0.20	0.25 ± 0.22	-0.88 ± 0.24	-0.19 ± 0.24	-0.27 ± 0.26		17	11	9
	10	0.84 ± 0.05	0.62 ± 0.10	0.74 ± 0.14	0.16 ± 0.16	0.67 ± 0.18	-0.02 ± 0.20	0.18 ± 0.23	-0.86 ± 0.24	-0.32 ± 0.27	-0.30 ± 0.27	-0.30 ± 0.31	17	10	9
1700	6	0.73 ± 0.04	0.87 ± 0.08	0.90 ± 0.11	0.73 ± 0.12	0.65 ± 0.13	0.55 ± 0.14	0.15 ± 0.14					36	14	0.1
	[7]	0.78 ± 0.04	0.87 ± 0.08	0.88 ± 0.11	0.64 ± 0.12	0.57 ± 0.13	0.27 ± 0.15	-0.13 ± 0.15	-0.76 ± 0.16				12	13	52
	8	0.78 ± 0.04	0.89 ± 0.08	0.88 ± 0.11	0.63 ± 0.12	0.54 ± 0.14	0.25 ± 0.15	-0.22 ± 0.17	-0.85 ± 0.17	-0.25 ± 0.17			10	12	60
	9	0.78 ± 0.04	0.89 ± 0.08	0.88 ± 0.11	0.63 ± 0.12	0.54 ± 0.14	0.25 ± 0.16	-0.22 ± 0.17	-0.84 ± 0.19	-0.23 ± 0.18	0.03 ± 0.21		10	11	51
	10	0.78 ± 0.04	0.89 ± 0.08	0.88 ± 0.11	0.61 ± 0.12	0.54 ± 0.14	0.25 ± 0.16	-0.19 ± 0.18	-0.83 ± 0.19	-0.15 ± 0.22	0.06 ± 0.21	0.14 ± 0.23	10	10	46

[a] Boxes indicate order chosen as necessary and sufficient.

V. INTERPRETATION OF THE RESULTS

The most striking characteristic of meson-baryon scattering below 1 or 2 BeV/c is the existence of resonances in the direct or s channel (see Fig. 17). As the total c.m. energy of the scattering system passes through a resonant energy, cross sections exhibit peaks, production and polarization angular distributions change rapidly, etc. In the analysis of such phenomena, a partial-wave amplitude having the isotopic spin, angular momentum, and parity of a resonant state is parameterized with the Breit-Wigner form; nonresonant amplitudes are assumed to be well-behaved, i.e., to vary relatively slowly with energy. The classic and most detailed instance of this type of analysis of K^-p scattering is that of Watson, Ferro-Luzzi, and Tripp[7] in their treatment of the $Y_0^*(1520)$. Data from all reaction channels were used. The nonresonant amplitudes were parameterized using a constant-scattering-length formalism.

With increasing momentum, more and more reaction channels are kinematically open, and the coupling of any one of them to resonances in the s channel is likely to be weak. At still higher momenta (several BeV/c), the "line spectrum" of resonant states is left behind and the "continuum" is reached. Here at least the 2-body and quasi-2-body reaction channels are dominated by peripheral mechanisms, i.e., by the exchange of particles or resonances in the t and u channels (see Fig. 17). Application of the usual conservation laws (excepting that of four momentum) severely restricts the possible exchange systems in these channels. For instance, in Fig. 17(c), the ρ meson has the lowest mass of those particles that can be exchanged, while in Fig. 17(d), no known particle has the appropriate quantum numbers $B = S = Q = +1$. Four momentum cannot be conserved at the vertices in these Yukawa-like exchanges, but, obeying a kind of Coulomb's law, the exchange particles of lowest mass dominate; they are closest to the "physical region." The angular momentum and parity of the exchanged system determines the polarization correlations. Indeed it is the experimental evidence on these correlations that points most strongly to the exchange of a

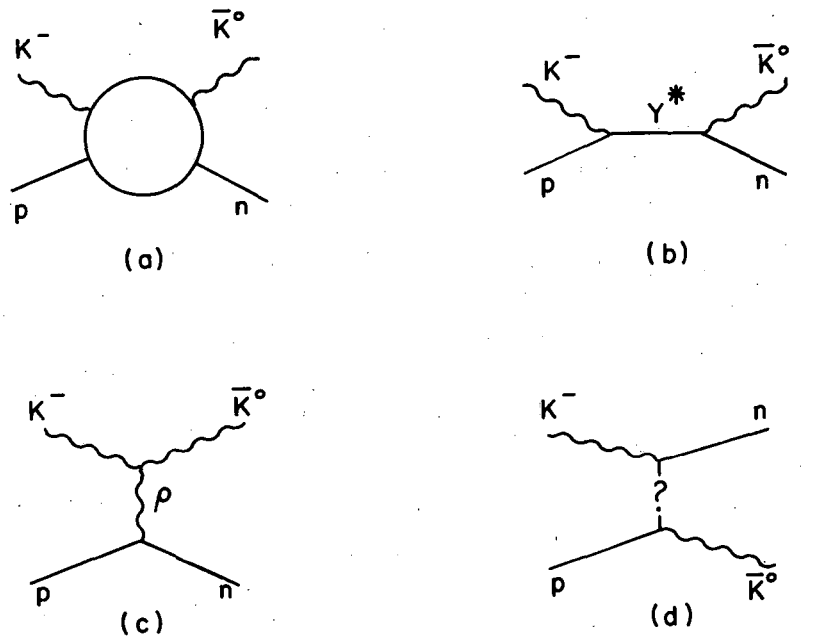

Fig. 17. (a) Interaction of the K^- and p through some mechanism (or combination of mechanisms) to produce $\bar{K}^0$ and n. The simplest s-, t-, and u-channel diagrams are shown in (b), (c), and (d), respectively.

system having definite quantum properties. The production angular distributions are determined primarily by the mass of the exchanged system; the spins of the particles enter in subordinate fashion. Exchange in the t channel leads to peaking of the production angular distributions in the forward direction; the smaller the exchanged mass and the higher the incident momentum, the sharper the peaking will be. Almost always the peaking of the experimental distributions is much sharper than predicted by the simple model. Various modifications to correct this deficiency have been proposed.[20]

In the following discussion it will become evident that a peripheral mechanism (t-channel effect) plays an important role, at least at the higher momenta of this experiment. However, this mechanism by itself is not sufficient to explain the data. It is probable that at least one of the partial-wave amplitudes can be associated with a Y^* resonant state (s-channel effect) having a mass above 2 BeV; this aspect of the results receives most attention. It remains to be seen whether or not the folding together of amplitudes corresponding to resonances in the s and t channels is sufficient to explain all aspects of the data. At present no complete analysis is attempted. Data on other channels, particularly on elastic scattering will be necessary for such an attack.[21] However, it is still possible to extract useful information. To do so it is first necessary to relate the properties of the differential cross sections and the behavior of the scattering amplitudes.

A. Scattering Amplitudes, Partial Waves, Resonant States, and Differential Cross Sections

The amplitude for scattering of spin-0 mesons on spin-1/2 baryons can be written

$$A(\theta) = f(\theta) + ig(\theta)\,\vec{\sigma}\cdot\vec{n}. \tag{7}$$

Here θ is the c.m. scattering angle, $\vec{\sigma}$ is the baryon spinor, and $\vec{n}$ is the unit vector normal to the production plane,

$$\vec{n} = \frac{\vec{q}_i \times \vec{q}_f}{|\vec{q}_i \times \vec{q}_f|}, \tag{8}$$

where $\vec{q}_i$ and $\vec{q}_f$ are the initial and final momenta in the c.m. system. The non-spin-flip and spin-flip amplitudes, $f(\theta)$ and $g(\theta)$, can be expanded in terms of partial-wave amplitudes $T_L^{\pm}$ each having orbital angular momentum = L, parity = $(-1)^L$, and spin J = L ± 1/2:[22]

$$f(\theta) = \lambda \sum_{L=0} \{(L+1)T_L^+ + LT_L^-\} P_L(\cos\theta)$$
$$g(\theta) = \lambda \sum_{L=1} (T_L^+ - T_L^-) P_L^1(\cos\theta) . \qquad (9)$$

The $T_L^{\pm}$ are energy-dependent. The angular dependence of $f(\theta)$ and $g(\theta)$ is contained in the ordinary and first-associated Legendre polynomials, $P_L(\cos\theta)$ and $P_L^1(\cos\theta)$, respectively.

The amplitudes are complex numbers. In the case of elastic scattering, each partial-wave amplitude can be expressed in terms of two real numbers, η and δ, as

$$T = \frac{\eta e^{2i\delta} - 1}{2i} = \frac{\eta \sin 2\delta}{2} + \frac{i(1 - \eta\cos 2\delta)}{2}, \qquad (10)$$

where $0 \leq \eta \leq 1$ and $0 \text{ deg} \leq \delta \leq 180 \text{ deg}$. Figure 18(a) shows the amplitude schematically. The restriction on η, which follows from the requirement of unitarity (conservation of probability), bounds the amplitude within a unit circle centered at i/2. Thus we have Im $T \geq 0$.

The optical theorem relates the total cross section (all channels) and the elastic-scattering amplitude:

$$\sigma_{\text{total}} = 4\pi\lambda \text{ Im } A(0 \text{ deg}). \qquad (11)$$

At $\theta = 0$ deg, the P_L are +1 and the P_L^1 are 0; hence A(0 deg) is f(0 deg). Equations (9) and (11) yield

$$\sigma_{\text{total}} = 4\pi\lambda^2 \sum_{\substack{\text{All} \\ \text{waves}}} (J + 1/2) \text{ Im } T. \qquad (12)$$

In general, the energy dependence of the partial-wave amplitudes is not known. However, the existence of a resonant state allows a simple and elegant parameterization of the relevant partial wave. The elastic amplitude is[23,24]

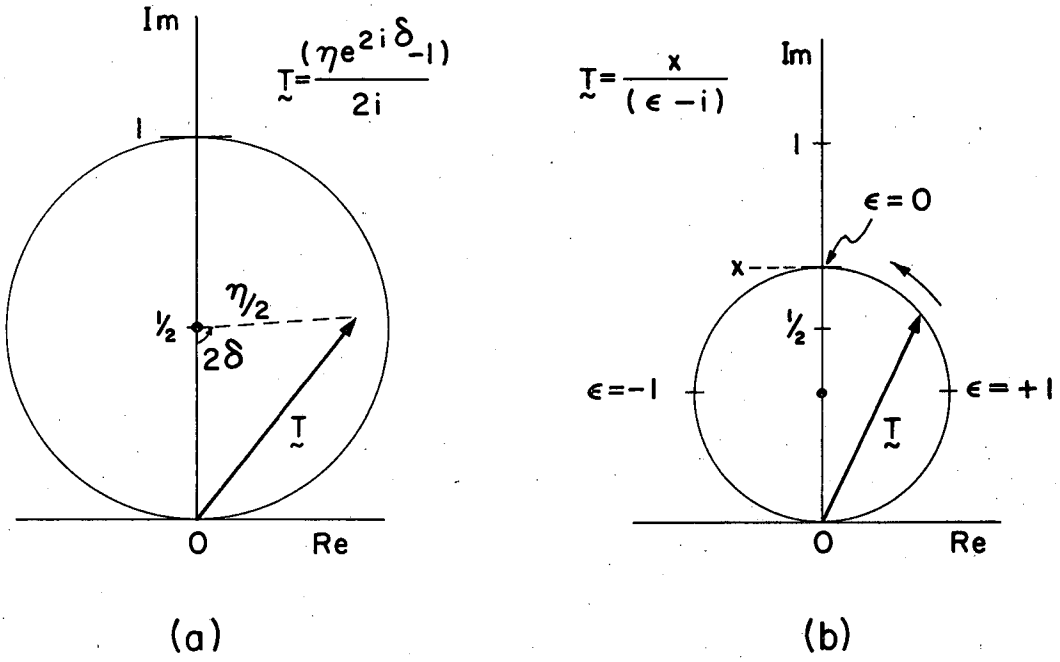

Fig. 18. (a) Unitarity bounds each (elastic) partial-wave amplitude within a circle of unit diameter. An amplitude $\underset{\sim}{T}$ is specified by two real numbers, conveniently η and δ. (b) A resonance amplitude is parameterized with the Breit-Wigner form, which specifies its energy dependence; with increasing energy the amplitude traverses a circle of diameter x in the counterclockwise direction.

$$T(\omega) = \frac{\omega_0 \Gamma_{el}}{(\omega_0^2 - \omega^2) - i\omega_0 \Gamma} . \qquad (13)$$

Here ω is the total c.m. energy, and ω_0 is the resonant-state energy; Γ_{el} and Γ are the elastic and total decay widths. (The widths are not constants, but are themselves energy-dependent. This is discussed below.) In general ω_0 is much greater than Γ. Then, within a few decay widths of ω_0, we have $\omega \cong \omega_0$ and $(\omega_0^2 - \omega^2) \cong 2\omega_0(\omega_0 - \omega)$. With the definitions

$$x = \Gamma_{el}/\Gamma \qquad (14a)$$

and

$$\epsilon = \frac{(\omega_0^2 - \omega^2)}{\omega_0 \Gamma} \cong \frac{\omega_0 - \omega}{\Gamma/2}, \qquad (14b)$$

Eq. (13) becomes

$$T(\omega) = \frac{x}{\epsilon - i} . \qquad (15)$$

Here x, called the elasticity, is the branching fraction into the elastic channel; ϵ is closely the difference $(\omega_0 - \omega)$, measured in half-widths. Figure 18(b) shows the amplitude schematically. To the extent that Γ_{el} and Γ have the same energy dependence, the amplitude traces a circle. The circle is traversed counter-clockwise as the energy increases.[25] Comparison of Fig. 18(a) and (b) shows that for $x > 1/2$ ($x < 1/2$), δ is 90 deg (0 deg) at $\omega = \omega_0$. The quantity η is not a constant of the amplitude; it can even pass through zero at resonance. The elasticity x is a more meaningful parameter; it is simply the diameter of the circle.

The energy dependence of the widths arises from two sources: 2-body phase space and an angular-momentum barrier effect. Phase space varies as q/ω. A parameterization of the angular-momentum barrier effect which is at least qualitatively correct is[23,26]

$$\left(\frac{q^2}{q^2 + X^2}\right)^L , \qquad (16)$$

where L is the orbital angular momentum, and X is a mass characterizing the radius of interaction. Then we have

$$\frac{\Gamma(\omega)}{\Gamma(\omega_0)} = \left(\frac{\omega_0}{\omega}\right) \cdot \left(\frac{q}{q_0}\right)^{2L+1} \cdot \left(\frac{q_0^2 + X^2}{q^2 + X^2}\right)^L . \tag{17}$$

For small X ($X^2 \ll q^2$), the radius of interaction is large and the barrier is weak; Γ is proportional to q. For large X, the radius of interaction is small and the barrier is strong; Γ is proportional to q^{2L+1}. Different reaction channels may require different radii of interaction.[27]

If the target baryon is unpolarized, the differential cross section is

$$\frac{d\sigma}{d\Omega} = |f(\theta)|^2 + |g(\theta)|^2 . \tag{18}$$

This can be expanded in a Legendre polynomial series:

$$\frac{d\sigma}{d\Omega} = \lambda^2 \sum_{n=0} B_n P_n(\cos\theta) . \tag{19}$$

If we expand the B_n in terms of the interferences between partial-wave amplitudes, we have

$$B_n = \sum_{i \leqq j} b_{ij}^n \, \underline{\mathrm{Re}}(T_i^* T_j)$$

$$= \sum_{i \leqq j} b_{ij}^n \, \vec{T}_i \cdot \vec{T}_j . \tag{20}$$

Here the amplitudes have been treated as complex numbers and as two-component vectors in turn. The unitarity condition implies $\vec{T}_i \cdot \vec{T}_j \leqq 1$. The numerical coefficients b_{ij}^n are given in Table IV.

The structure of Table IV is quite simple:

(a) The interference between two partial waves having angular momenta J_1 and J_2 and even (odd) relative parity contributes to those B_n with even (odd) n and $(J_1 + J_2) \geqq n \geqq |J_1 - J_2|$.

(b) The expansion of the production angular distribution is invariant under the simultaneous interchange of parities of all states (Minami ambiguity), i.e., $S_{1/2} \leftrightarrow P_{1/2}$, $P_{3/2} \leftrightarrow D_{3/2}$, etc. Interference terms that are the (Minami) transforms of one another are grouped together in the table.

Table IV. Legendre polynomial coefficients, b_{ij}^n, for the partial-wave expansion for spin-0 scattering on spin-$\frac{1}{2}$:

$$\frac{d\sigma}{d\Omega} = \lambda^2 \sum_n B_n P_n(\cos\theta), \qquad B_n = \sum_{i \leq j} b_{ij}^n \, \underline{\mathrm{Re}}\,(T_i^* T_j),$$

where the $T_i (= L_{2J})$ are partial-wave amplitudes.

	Expansion coefficients B_n							
$T_i\ T_j$	B_0	B_1	B_2	B_3	B_4	B_5	B_6	B_7
$S_1\ S_1$ and $P_1\ P_1$	1							
$P_3\ P_3$ and $D_3\ D_3$	2		2					
$D_5\ D_5$ and $F_5\ F_5$	3		24/7		18/7			
$F_7\ F_7$ and $G_7\ G_7$	4		100/21		324/77		100/33	
$S_1\ P_1$		2						
$P_3\ D_3$		4/5		36/5				
$D_5\ F_5$		18/35		16/5		100/7		
$F_7\ G_7$		8/21		24/11		600/91		9800/429
$S_1\ P_3$ and $P_1\ D_3$		4						
$S_1\ D_3$ and $P_1\ P_3$			4					
$S_1\ D_5$ and $P_1\ F_5$			6					
$S_1\ F_5$ and $P_1\ D_5$				6				
$S_1\ F_7$ and $P_1\ G_7$				8				
$S_1\ G_7$ and $P_1\ F_7$					8			
$P_3\ D_5$ and $D_3\ F_5$		36/5		24/5				
$P_3\ F_5$ and $D_3\ D_5$			12/7		72/7			
$P_3\ F_7$ and $D_3\ G_7$			72/7		40/7			
$P_3\ G_7$ and $D_3\ F_7$				8/3		40/3		
$D_5\ F_7$ and $F_5\ G_7$		72/7		8		40/7		
$D_5\ G_7$ and $F_5\ F_7$			8/7		360/77		200/11	

(c) All b_{ij}^{n} are positive. Negative contributions to the B_n come from interferences that are negative, either in themselves or because of negative signs in the isotopic spin decomposition of the scattering amplitude.

From (a) it follows that interferences between states having different spin and (or) parity cannot contribute to B_0:

$$B_0 = \sum_{\substack{\text{All} \\ \text{waves}}} a_i |T_i|^2. \tag{21}$$

The a_i are just $(J + 1/2)$. Integration of $d\sigma/d\Omega$ over production angles $d\Omega$ yields $\sigma = 4\pi\lambda^2 B_0$. The factor $\pi\lambda^2$ is roughly a measure of the cross-sectional area of interaction in a single orbital angular-momentum state; this decreases with increasing c.m. momentum. Consequently B_0, rather than σ, better exhibits changes in the magnitudes of the partial-wave amplitudes.

Table IV is written for scattering in a pure isotopic spin state. For any particular channel, the amplitudes $A(\theta)$, $f(\theta)$, $g(\theta)$, and the T_i can be further expanded (all in the same way) in terms of pure isotopic-spin amplitudes. Equation (4) gives this decomposition for K^-p charge-exchange scattering. In this case, with the angular-distribution expansion normalized as in Eq. (3) (now σ is $\pi\lambda^2 B_0$), an entry T_i in Table IV is to be read as the difference between the $I = 0$ and $I = 1$ amplitudes, i.e., $S_{1/2} \rightarrow (S^1_{1/2} - S^0_{1/2})$, etc., where the superscripts represent isotopic spin. Since the maximum length of the difference between two vectors lying in a unit circle is one, there remains $\vec{T}_i \cdot \vec{T}_j \rightarrow (\vec{T}^1_i - \vec{T}^0_i) \cdot (\vec{T}^1_j - \vec{T}^0_j) \leqq 1$. Since the isotopic-spin amplitudes enter into the K^-p charge-exchange cross section in a symmetric way, isotopic spin cannot be determined on the basis of this channel alone.

The information derived from differential cross sections is not in itself sufficient to fix the partial-wave amplitudes. Table IV shows that if the first n amplitudes $S_{1/2}$, $P_{1/2}$, $P_{3/2}$, ... etc. are present, the n coefficients B_0 through $B_{(n-1)}$ are affected. Conversely, if the

nth coefficient is not zero, the presence of n partial-wave amplitudes must be considered. Thus a cross section described by n numbers denotes 2n unknown quantities. (Polarization data, when accessible, provide n-1 additional constraints. In the case of elastic scattering, the optical theorem adds a further constraint.) The number of unknowns is further multiplied by the number of isotopic spin states that contribute to the reaction. Any attempt to fully analyze the scattering amplitudes must reduce the number of free parameters by postulating specific forms for their energy dependence.

B. Behavior of the Coefficients

The expansion coefficients B_n from this and other experiments are displayed in Figs. 19 and 20. Where the published expansions are in powers of $\cos\theta$, the data have been refit with the Legendre polynomial expansion. Where necessary, coefficients have been renormalized to coincide with our conventions. If only the integrated cross section is available, or the differential cross section is not well determined, only B_0 can be plotted.

Generally the highest Legendre polynomial required at each momentum can be determined from the plots of the coefficients. Thus at 1.22 BeV/c, the expansion series including $P_6(\cos\theta)$ is both necessary and sufficient because B_6 is the highest of the B_n to differ significantly from zero. (In this case, coefficients B_0 through B_6 are taken from the $n_{max} = 6$ fit, while B_7 is taken from the $n_{max} = 7$ fit.)

Polynomials higher than $P_7(\cos\theta)$ probably are necessary at one momentum, 1.80 BeV/c,[13] where the probability that the series through $P_7(\cos\theta)$ is sufficient is only about 2%. There is considerable requirement for $P_9(\cos\theta)$ and $P_{10}(\cos\theta)$. Coefficients B_9 and B_{10} are negative. Together these terms reproduce a sharp dip in the forwardmost bin of the differential cross section, while elsewhere their effects largely cancel one another. Aside from the forward dip, the cross section is quite similar to that at 1.70 BeV/c. This is apparent from the near equality of the coefficients B_0 through B_7 at the two momenta.[28] The B_{10} denotes an interference like $H_{9/2} \cdot H_{11/2}$. (Two waves are required

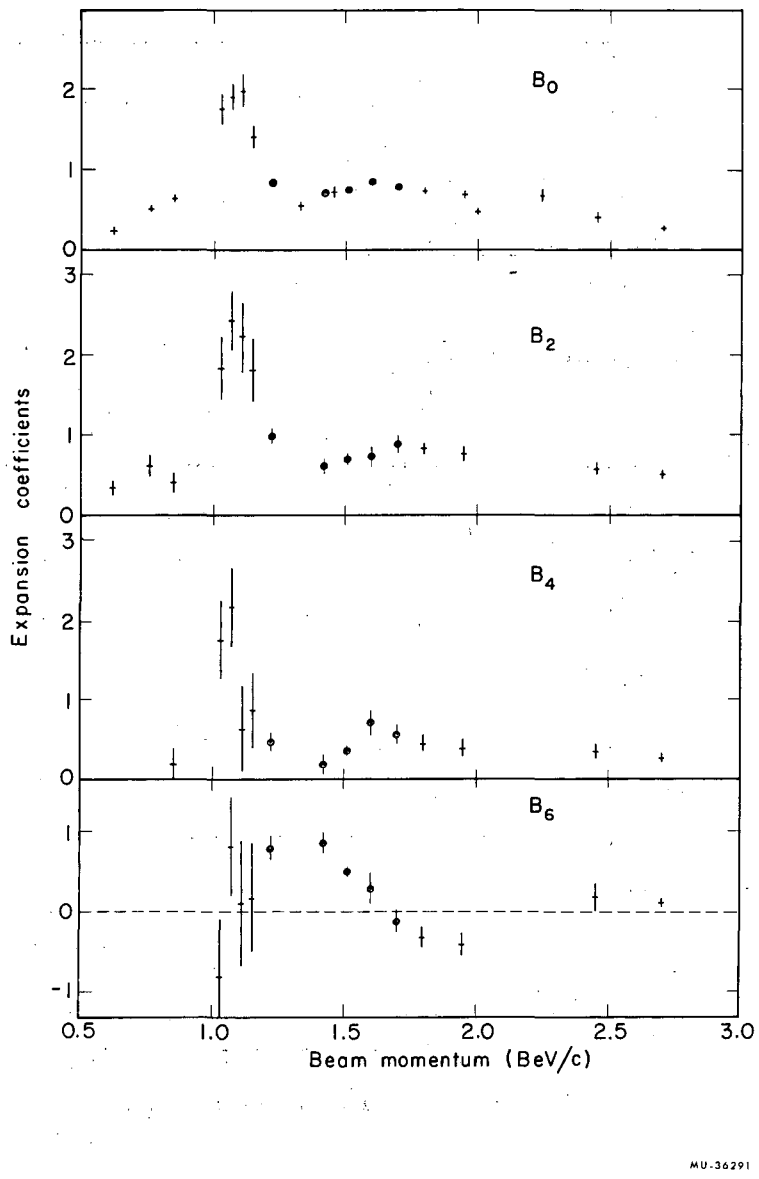

Fig. 19. Even expansion coefficients, B_n, of the differential cross sections. The normalization is $d\sigma/d\Omega = (\lambda^2/4) \sum B_n P_n(\cos\theta)$. (The references may be obtained by comparison with Fig 10.)

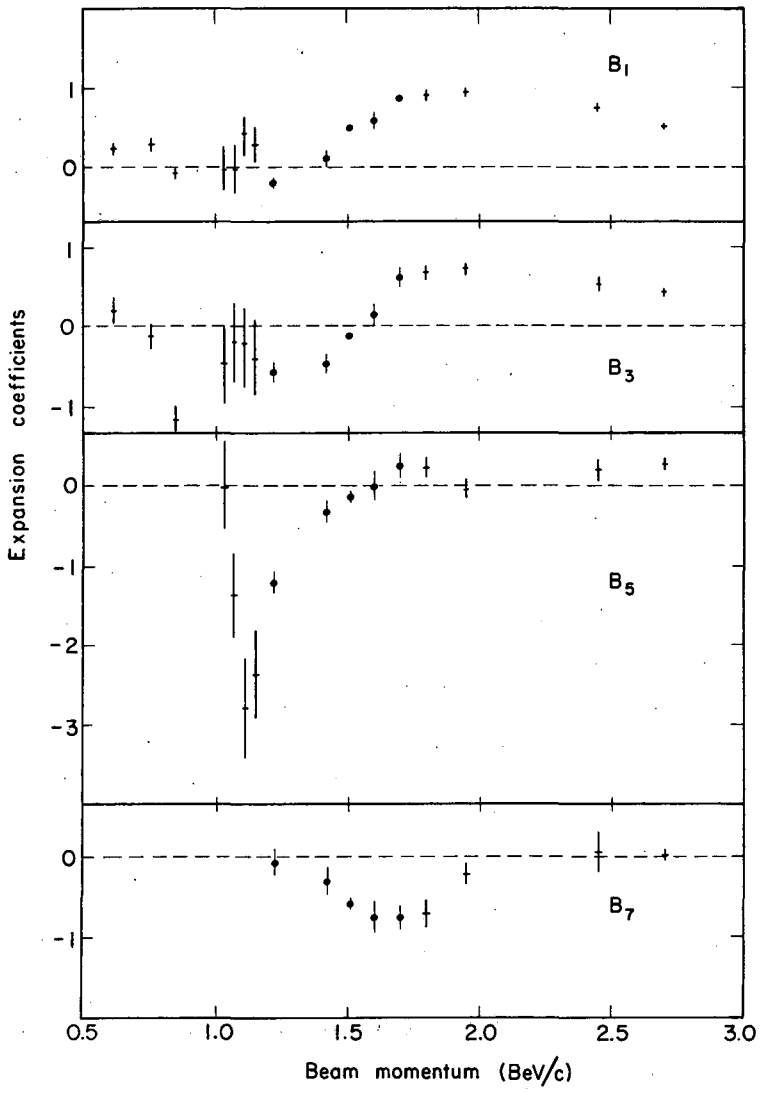

Fig. 20. Odd expansion coefficients, B_n, of the differential cross sections.

since B_{10} is negative.) The B_9 denotes an interference like $G_{7/2} \cdot H_{11/2}$. At 1.95 BeV/c[14] the series through $P_7(\cos\theta)$ is again sufficient, so the effect is quite narrow. It might be expected that the high angular-momentum amplitudes would interfere with lower ones to disturb the smooth variation of at least some of the lower coefficients over a similarly narrow momentum range; this is clearly not the case. Hereafter, the possible effects of amplitudes with $J > 7/2$ are not considered.

Several general characteristics of the behavior of the coefficients warrant observation:

(a) Around 1.0 BeV/c, the coefficients are dominated by the $Y_1^*(1765)$ and $Y_0^*(1815)$ resonant states.[29] Both of these have $J = 5/2$. They have opposite parities. Though the evidence is not yet conclusive, the $Y_1^*(1765)$ has been taken to be $D_{5/2}$ and the $Y_0^*(1815)$, $F_{5/2}$. Both resonances are coupled strongly to the $\bar{K}N$ system. The interference between the two causes the marked peak in B_5. Effects of these amplitudes extend at least past 1.2 BeV/c.

(b) B_0 is fairly constant between 1.2 and 2.0 BeV/c before it falls off at higher momenta. Over the same interval, B_7, B_6, and to a lesser degree some of the lower coefficients display activity centered around 1.5 to 1.8 BeV/c that does not appear to be correlated with the asymptotic behavior of the coefficients at high momenta. In particular, around 2.5 BeV/c there is little requirement for $P_6(\cos\theta)$ and none for $P_7(\cos\theta)$.

(c) Around 1.4 BeV/c, coefficients B_1, B_3, and B_5 pass from negative to positive values, thus reflecting the shift of the angular distribution from backward to forward peaking. The coefficients of the lower even polynomials are relatively stable.

(d) Around 2.5 BeV/c, all coefficients are positive, and thus all polynomials add constructively to the forward peak. From 2.45 to 2.70 BeV/c, B_0, B_1, B_2, and B_3 decrease, while B_4 and B_5 increase. At 2.45 BeV/c, the expansion series including $P_5(\cos\theta)$ is probably sufficient. At 2.70 BeV/c, the series including $P_6(\cos\theta)$ is necessary and sufficient. The coefficients reflect the increasing sharpness of the forward peak. In all probability the peaking persists at all higher momenta.[30]

The last two observations indicate that a peripheral mechanism plays a role down to at least 1.5 BeV/c. The angular distribution predicted at 1.70 BeV/c by the exchange of a vector boson with the mass and couplings of a ρ is included in Fig. 15.[31] As expected, the peak in the theoretical curve is much broader than that in the experimental distribution. However, the peak in the experimental distribution still is quite broad below 2.0 BeV/c. The requirement for $P_6(\cos\theta)$ and $P_7(\cos\theta)$ is due rather to the undulations in the angular distributions than to the sharpness of the forward peak. [The sharper backward peak at 1.22 BeV/c requires only $P_6(\cos\theta)$.] Experimentally, the forward peak becomes narrower with increasing momentum. It seems unlikely that the properly modified peripheral model -- whatever form this eventually takes -- will necessitate higher terms in the Legendre polynomial series below than above 2.0 BeV/c. Consequently, it can reasonably be inferred from the behavior of the coefficients B_6 and B_7 above 2.0 BeV/c that below 2.0 BeV/c the "projections" of the suitably modified t-channel exchange amplitude on the (s-channel) partial-wave amplitudes with $J > 5/2$ are negligible. This iterates the conclusion of observation (b), and attributes the behavior of B_6 and B_7 between 1.0 and 2.0 BeV/c to some other mechanism than a peripheral one.

A $J = 7/2$ amplitude is first clearly in evidence at 1.22 BeV/c; the substantial B_6 requires it. Below this momentum the data are not sufficient to confirm or exclude its presence. The B_7 above 1.4 BeV/c signifies the presence of $J = 7/2$ amplitudes having both parity values. Some measure of the importance of these amplitudes can be obtained from the magnitude of B_7, which consists entirely of the $F_{7/2} \cdot G_{7/2}$ interference. The simple inequalities

$$(|\vec{F}_{7/2}|^2 + |\vec{G}_{7/2}|^2) \geqq 2|\vec{F}_{7/2}| \cdot |\vec{G}_{7/2}| \geqq |2\,\vec{F}_{7/2} \cdot \vec{G}_{7/2}| \quad (22)$$

and the coefficients of Table IV yield

$$|\vec{F}_{7/2}| \cdot |\vec{G}_{7/2}| \geqq 0.044\,|B_7| \quad (23)$$

and

$$B_0 \text{ from } J = 7/2 \text{ amplitudes} \geqq 0.35\,|B_7|\,. \quad (24)$$

In Eq. (23) the equality obtains if the two amplitudes have the same phase. In Eq. (24) the equality obtains only if the magnitudes also are equal. Around 1.6 to 1.8 BeV/c the magnitude of B_7 is approximately equal to B_0, so the $J = 7/2$ amplitudes account for at least a third of the cross section. In the same region, Eq. (23) places a lower limit of 0.18, or 18% of the unitary limit, on the magnitude of the larger of the two amplitudes. (In these equations, $F_{7/2}$ is $F^1_{7/2} - F^0_{7/2}$, etc. The limits apply whether or not one or the other of the isotopic spin states dominates each of $F_{7/2}$ and $G_{7/2}$.)

The squares of the $J = 7/2$ amplitudes contribute to B_6 (see Table IV). These contributions are always positive, and appear also in B_0, enlarged by 32%. Above 1.7 BeV/c, the experimental values of B_6 are negative; between 1.2 and 1.5 BeV/c, B_6 is too large to be consistent with B_0 if the only contributions to B_6 are the squares of the $J = 7/2$ amplitudes. The only other terms contributing to B_6 are the $F_{5/2} \cdot F_{7/2}$ and $D_{5/2} \cdot G_{7/2}$ interferences. Evidently one or both of these play important roles.

As it is difficult to attribute the behavior of some of the expansion coefficients around 1.5 to 1.8 BeV/c to a peripheral mechanism, it is natural to investigate the possibility that it is due to a resonant state in the s channel. The preceding observations would suggest that if such a state exists, it has $J = 7/2$. In the study of πN scattering one can often fix the quantum numbers of an N^* by its interference with the N^* below it.[32] The relative quantum numbers of the $Y^*(1765)$ and the $Y^*(1815)$ are determined in the same way.[29] With this in mind, the conclusion of the previous paragraph is suggestive. There are strong $J = 5/2$ resonant amplitudes around 1.0 BeV/c and moderate $J = 7/2$ amplitudes around 1.7 BeV/c. An interference term, $\vec{T}_i \cdot \vec{T}_j$, between two widely separated resonances is dominated by the real parts of the resonant amplitudes, since at any energy at least one of the amplitudes is predominantly real. The interference has the shape of a curve drawn through B_6 (see Fig. 19). The positions of the resonances are close to the "nodes," near which one or the other of the amplitudes is purely imaginary, and its real part changes sign. Close

to the lower node is the $Y_0^*(1815)$. Interference with this $F_{5/2}$ resonance shows the other resonance to be an $I = 1$, $F_{7/2}$ Y^* with a mass of about 2065 MeV (corresponding to 1.60 BeV/c). The sign of B_6 determines the relative isotopic spins. Here the condition that all resonant amplitudes traverse circles in the same (counter-clockwise) direction is important.[33]

The validity of this interpretation rests on the assumption that the other terms that can contribute to B_6 do not alter its qualitative features. The situation may in fact be much more complicated. However, to proceed much further with the limited data, one must provisionally assume simplicity and see where that leads.

The contribution of the two resonant amplitudes to B_6 is

$$b_6 = \frac{100}{33}\left(|\vec{F}_{7/2}|^2 - 6\,\vec{F}_{5/2}\cdot\vec{F}_{7/2}\right). \tag{25}$$

The negative sign of the second term comes from the isotopic spin expansion. By using Eq. (15), Eq. (25) becomes

$$b_6 = \frac{100}{33}\left[\frac{x'^2}{1+\epsilon'^2} - \frac{6xx'(1+\epsilon\epsilon')}{(1+\epsilon^2)(1+\epsilon'^2)}\right], \tag{26}$$

where unprimed (primed) quantities refer to the $J = 5/2$ (7/2) amplitude. The contribution to B_6 of the second term in Eq. (26) is positive over most of the distance between the two resonances, because there $\epsilon\epsilon'$ is negative. The $Y_0^*(1815)$ causes large bumps in the $\bar{K}N$ cross sections, and the $Y_1^*(2065)$ does not; thus x is large and x' is not. Then the second term will dominate. This has already been seen to be necessary if the behavior of B_6 is to be explained in this way. The width of the $Y_0^*(1815)$ is small compared to the range over which B_6 is consequential; thus the width of the $Y_1^*(2065)$ is large.

One can estimate the width and elasticity of the hypothesized Y^* by fitting b_6, given by Eq. (26), to the experimental points $B_6^i \pm \delta B_6^i$. The function

$$\chi^2 = \sum_i \left\{\frac{B_6^i - b_6^i}{\delta B_6^i}\right\}^2 \tag{27}$$

has been minimized with respect to Γ' while the other resonance parameters were held fixed at values within ranges compatible with the magnitude and shape of B_0.[34] Two curves so generated are shown in Fig. 21. Also shown are their "projections" onto B_0, given by

$$3\left|\vec{F}_{5/2}\right|^2 + 4\left|\vec{F}_{7/2}\right|^2 = \frac{3x^2}{1+\epsilon^2} + \frac{4x'^2}{1+\epsilon'^2} . \qquad (28)$$

Certainly other amplitudes are present, so not all of B_0 can be given up to the two resonant amplitudes. Both sets of curves use $\omega_0 = 1825$ MeV (somewhat above the nominal mass), $\omega_0' = 2065$ MeV, $x = 0.7$, $x' = 0.35$, and X [in Eq. (17)] = 350 MeV.[26] The solid curves have $\Gamma = 50$ MeV and $\Gamma' = 180$ MeV; the dashed curves have $\Gamma = 70$ MeV and $\Gamma' = 185$ MeV. The width Γ' is fairly insensitive to small changes in the values of the other parameters. Since X^2 is smaller than q^2 (for q, see Fig. 10), the energy dependence of the widths is more closely proportional to q than to $q^{2L+1} = q^7$. Since the second term of Eq. (26) dominates B_6, the principal effect of a small change in the elasticities is to scale the B_6 curves proportionately.

The data included in Fig. 21 favor a width closer to 70 than to 50 MeV for the $Y_0^*(1815)$. However, an extended K^- run at CERN, over the laboratory momentum interval 0.80 to 1.20 BeV/c, gives as a preliminary result a width of 45 ±5 MeV.[35]

At 1.22 and 1.42 BeV/c, agreement between the fitted curves and the experimental measurements of B_6 is poor. This is due mainly to the limitations placed on the elasticities of the resonances by the magnitude of B_0. The upper limit on x' is about 0.35. It is most natural to invoke a small I = 1, $F_{5/2}$ amplitude to interfere with the $F_{7/2}$ resonant amplitude in order to make up the discrepancy in B_6. Judging by B_7, it is probable that the $G_{7/2}$ amplitude is not significant below 1.42 BeV/c.

At resonance, the imaginary part of the elastic-scattering resonant amplitude is equal to the elasticity. By the optical theorem, Eq. (12), the resonance causes an enhancement in the total cross section equal to $4\pi\lambda^2 a(J + 1/2)x$, where a is an isotopic spin factor.

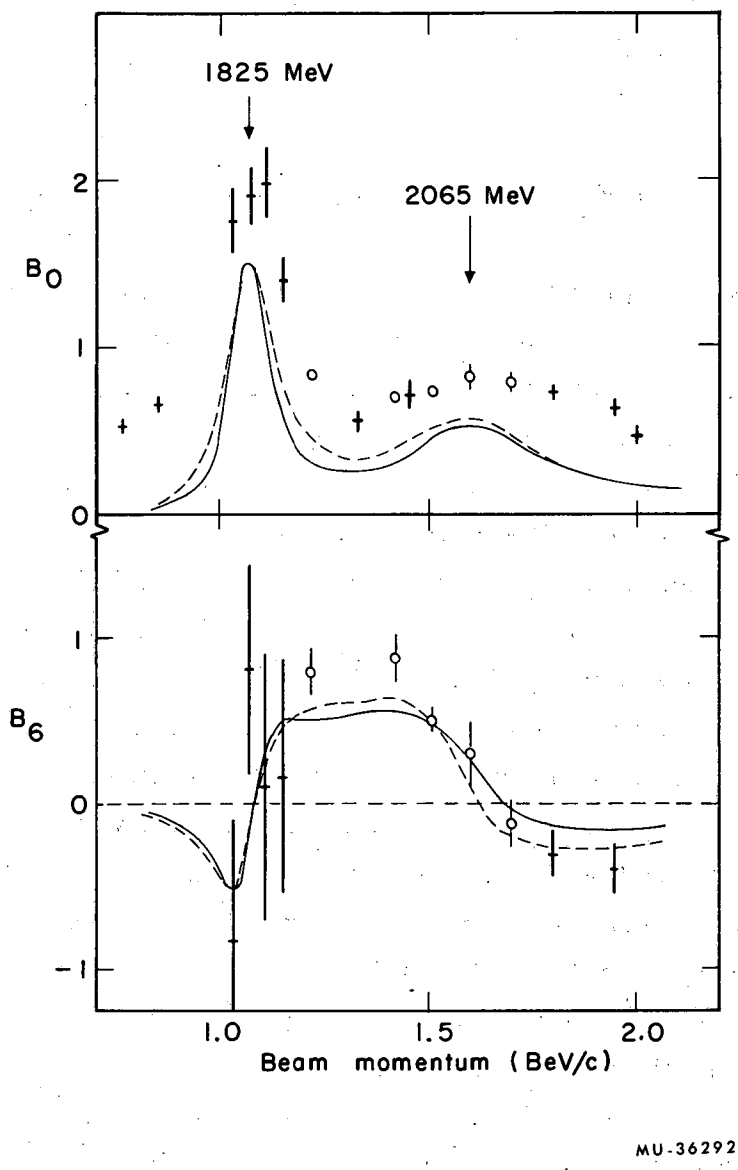

Fig. 21. B_0 and B_6 and some curves obtained by fitting the experimental B_6 with the interference term given by Eq. (26). Both curves are drawn for ω_0 = 1825 MeV, ω_0' = 2065 MeV, x = 0.70, x' = 0.35, and X = 350 MeV. The solid curves are drawn for Γ = 50 MeV and Γ' = 180 MeV; the dashed curves are drawn for Γ = 70 MeV and Γ' = 185 MeV.

At 2065 MeV in the $\bar{K}N$ system, and with $J = 7/2$, $4\pi\lambda^2(J + 1/2)$ is 37 mb. An $I = 1$ resonance with an elasticity of 0.35 will cause an enhancement of 6.5 mb in the total K^-p cross section and twice this in the total K^-n cross section. There is indeed a broad enhancement of a few mb, situated at about the correct energy, in the total K^-p cross section.[36] It is difficult to estimate accurately how much of the cross section should be allotted to the enhancement rather than to background. There is relatively little data on the K^-n cross section, but what there is shows no evidence of structure.[36] This is perhaps not so damaging to the model as it would appear. There is a similar problem with regard to the $Y_1^*(1765)$; at 940 MeV/c there should be a 30-mb hump in the K^-n cross section, but nothing of this magnitude is suggested by the limited data.[36,37] It is quite difficult to extract accurately the K^-n cross section from measurements of the K^-d cross section. The subtractions to be made in order to account for the presence of the proton are uncertain; any structure in the K^-n cross section is partially erased by the internal momentum of the nucleons.[29]

Overall, the existing data are in accord with the existence of the proposed resonance, though certainly more complicated explanations could be proposed. There is other, independent, evidence for the existence of Y^*'s in the interval between 1850 and 2200 MeV:

(a) Blanpied et al. have studied K^+ production in γp reactions.[38] Assuming the dominant mode of production to be the 2-body reaction $\gamma + p \rightarrow K^+ + Y^*$, they find evidence for a $Y^*(2020)$ with a width of about 120 MeV. The statistics are quite limited. There is no evidence pertaining to the quantum numbers (I, J^P).

(b) Bock et al. have studied hyperon production in $\bar{p}p$ reactions, with a $\bar{p}$ laboratory momentum equal to 5.7 BeV/c.[39] The reaction channels $\bar{\Lambda}\bar{K}N$, $\bar{\Lambda}\bar{K}N\pi$, $\bar{\Sigma}\bar{K}N$, $\bar{\Sigma}\bar{K}N\pi$, and their charge conjugates are of particular interest: the invariant mass plot of the $\bar{K}N$ and $\bar{K}N\pi$ systems has a peak at 2100 MeV which "exceeds 3 standard deviations" above background; the width is less than 40 MeV. The peak comes almost entirely from the neutral systems, which is weak evidence for $I = 0$. There is also some evidence for a $Y_1^*(1940)$.

(c) Preliminary results of a study by Eberhard and Shively[40] of the reaction $K^- + p \rightarrow \Sigma^{\pm} + \pi^{\mp} + \pi^+ + \pi^-$, for K^- laboratory momenta from 2.45 and 2.7 BeV/c, show a peak in the invariant mass plot of the $\Sigma^+\pi^+\pi^-$ system when this is produced peripherally against the other π^-. The peak is at 2070 MeV and has a width of about 80 MeV. The $\Sigma^+\pi^+\pi^-$ system can have I = 1, 2, or 3, but the last of these cannot be reached by the production process.

(d) In the preliminary study of the Λ events from this experiment, Stevenson et al.[1] showed that the qualitative features of the production and polarization angular distributions from the pure I = 1 reaction $K^- + p \rightarrow \Lambda + \pi^0$ were reproduced by a model consisting of the exchange of an $F_{7/2}$ $Y_1^*(2030)$ in the s channel, together with other appropriate exchanges in the s, t, and u channels.

It is unfortunate that there is not better agreement among the various experimental indications of resonant states. Either the situation is quite complicated or, more probably, some of the data are deceptive with regard to the mass and (or) the width of the state they reveal. The implications of theory are discussed below.

Many partial-wave amplitudes can contribute to the lower expansion coefficients, and it seems impossible to extract much additional useful information from them. However, one further inference can perhaps be drawn from the coefficient B_7, if indeed the $F_{7/2}$ amplitude is dominated by an I = 1 resonance. Since B_7 is negative across the region where the resonant amplitude is predominately imaginary, at least the imaginary part of the $G_{7/2}$ amplitude must be dominated by the I = 0 state. The possible significance of this will appear below.

C. Theoretical Particle Spectroscopy

An $F_{7/2}$ baryon, the $N^*(1920)$, is already known. It has isotopic spin 3/2 and decays strongly into π + N, both of which are members of SU(3) octets.[41] The only irreducible representations in the supermultiplet product

$$8 \times 8 = 1 + 8 + 8 + 10 + \overline{10} + 27 \qquad (29)$$

that contain an $N^*_{3/2}$ are the 10 and the 27. Both of these also contain a Y^*_1.

According to the Chew-Frautschi extention of the concept of Regge trajectories to particle phenomenology,[42] the $N^*_{3/2}(1920)$ is the recurrence of the $N^*_{3/2}(1238)$. The $N^*_{3/2}(1238)$ belongs to the decuplet which contains also the $Y^*_1(1385)$, the $\Xi^*_{1/2}(1530)$, and the $\Omega^-(1675)$. Since one member of the decuplet has a recurrence, the others should also. A $Y^*_1(2065)$ falls naturally into this scheme as the recurrence of the $Y^*_1(1385)$.

The masses of the isotopic multiplets within an SU(3) supermultiplet are related by the formula due to Okubo,[43]

$$m = m_0 + \alpha Y + \beta \{I(I + 1) - Y^2/4\} , \qquad (30)$$

where Y is the hypercharge. For the members of a decuplet, we have $I = 1 + Y/2$, so that Eq. (30) reduces to $m = \alpha' + \beta' Y$, and the mass splittings between members are equal. For the decuplet containing the $N^*_{3/2}(1238)$, agreement between theory and experiment is spectacular; if one uses the best values (rather than the nominal ones) for the masses,[5] the splittings are 146, 147, and 146 MeV, respectively.

A Chew-Frautschi diagram plots J versus m^2. The path of a trajectory on the plot is determined experimentally by its manifestations as particle and (or) resonant states. The $N^*_{3/2}(1238)$ and the $N^*_{3/2}(1920)$ determine one trajectory. To estimate the masses of recurrences, one usually assumes that the slopes of neighboring trajectories are equal. This method gives, for the other members of the decuplet containing the $N^*_{3/2}(1920)$, masses of 2020, 2124, and 2232 MeV. The splittings are 100, 104, and 112 MeV, respectively. It is not possible to have equal slopes (versus m^2) and retain equal spacing (in m). Since the members of a supermultiplet are manifestations of a single entity, it is perhaps more sophisticated to associate a single trajectory with each supermultiplet, rather than with each multiplet. Splittings from the "supertrajectory" should then obey the mass formula. It is not evident how the magnitude of the splitting at one occurrence of a super-trajectory should be related to that at another. Certainly the finding of a $F_{7/2}$ Y^*_1

anywhere in the interval 2000 to 2100 MeV represents a triumph for theory. Experimentally, the mass difference 2065-1920 = 145 MeV is identical to the splitting in the low-lying decuplet, though if one considers the uncertainties in the mass determinations of the $F_{7/2}$ states, it is not clear how meaningful this apparent equality is.

In exact SU(3), the decay of a decuplet into two octets is characterized by a single coupling constant, g_0. Specific couplings, such as $N^*_{3/2} \rightarrow \pi + N$, are related to g_0 by Clebsch-Gordan coefficients;[44] thus, for example, we have

$$g(N^*_{3/2}, \pi N) = g_0/(2)^{1/2} \tag{31}$$

and

$$g(Y^*_1, \bar{K}N) = g_0/(6)^{1/2} . \tag{32}$$

The partial widths are proportional to the squares of the coupling constants, so that

$$\Gamma(N^*_{3/2}, \pi N) = 3\Gamma(Y^*_1, \bar{K}N) . \tag{33}$$

These relations can be modified with Eq. (17) to include the phase-space and angular-momentum-barrier effects arising from the mass differences within supermultiplets. Results of the calculations of the $N^*_{3/2}(1920)$ and the $Y^*_1(2065)$ are given in Table V. Input to the calculation is $\Gamma(N^*_{3/2}, \pi N)$, which is about 120 MeV. The total width of the $N^*_{3/2}(1920)$ is about 200 MeV.[45] To the extent that mass differences can be neglected, the total width of the $Y^*_1(2065)$ should be the same. The results of Table V show that effects of the mass differences do not appreciably alter this predicted value. Thus the experimental result, about 180 MeV, is in accord with the theoretical prediction. Finally, the predicted value of the elasticity, which is $\Gamma(Y^*_1, \bar{K}N)$ divided by the total width, is about 0.2. This is somewhat lower than the experimental result, about 0.35.

The Σ, the $Y^*_0(1405)$, and the $Y^*_0(1520)$ should recur as Y^*'s in the mass interval between 1850 and 2150 MeV. The quantum numbers (I, L_J) will be $(1, F_{5/2})$, $(0, D_{5/2})$, and $(0, G_{7/2})$, respectively. On

Table V. Partial widths, according to exact SU(3) modified for phase-space and angular-momentum barrier effects, for the decay of the $N^*_{3/2}$ and Y^*_1 members of the $7/2^+$ decuplet into the 0^- meson and $1/2^+$ baryon octets.

Resonance	Decay	q (MeV/c)	$f^a \times 10$	$(C\text{-}G)^{2\,b}$	Γ (MeV)
$N^*_{3/2}(1920)$	πN	723	2.0	1/2	120 (input)
	$K\Sigma$	435	0.5	1/2	30
					150 (of 200)
$Y^*_1(2065)$	$\bar{K}N$	727	1.9	1/6	38
	$\pi\Lambda$	725	1.9	1/4	57
	$\pi\Sigma$	675	1.6	1/6	32
	$\eta\Sigma$	525	0.8	1/4	24
	$K\Xi$	435	0.5	1/6	10
					161

[a] The phase-space and angular-momentum barrier factor [Eq. (17), with X = 350 MeV].

[b] The Clebsch-Gordan coefficient, squared.

the basis of calculations similar to those of the preceding paragraph, the Σ recurrence is expected to be only weakly coupled to the $\bar{K}N$ channel.[46] It has been deduced from the experimental results that the $G_{7/2}$ partial-wave amplitude is present in appreciable magnitude, and is probably dominated by the I = 0 state.

Overall, agreement between theory and experiment is good, especially considering the uncertainties that are present in both approaches.

D. Summary and Conclusions

The Legendre-polynomial series expansions of the angular distributions clearly display the presence of $F_{7/2}$ and $G_{7/2}$ partial waves. It is difficult to associate these amplitudes with a peripheral mechanism. It is probable that the $F_{7/2}$ amplitude signifies a Y_1^* with a mass of about 2065 MeV, a width of about 180 MeV, and an elasticity of about 0.35. If this is so, then the $G_{7/2}$ amplitude is probably dominated by the I = 0 state. This interpretation is in accord with theory. It rests on the assumption that the coefficient of $P_6(\cos\theta)$ is dominated by interference of the $F_{7/2}$ amplitude with the $Y_0^*(1815)$. A judgment as to the extent of the validity of this picture must await further information about the other 2-body channels.

ACKNOWLEDGMENTS

Thanks are due to Professor Luis W. Alvarez, whose efforts have provided the structure within which this work was done, and to the many members of his group, largely anonymous, who have made this work possible.

The beam was designed and built under the direction of Professor Harold K. Ticho (U. C. L. A.). Much of the organization of the processing of the data was done by Dr. Stanly G. Wojcicki. To him, and to Professors Donald H. Miller, M. Lynn Stevenson, and Robert D. Tripp are due thanks for the physics which they have taught me. In one way or another, the work has been influenced by my association with Drs. Jared Anderson, Richard Hubbard, and Joseph Schwartz.

The scanning work particular to this experiment was done by Josephine Canada Cochran and Reginald Paradis. The accuracy of the results is in large part due to their considerable efforts. Catherine G. Plasil did much of the work of keeping track of the progress of the events during film handling and computer processing. Roger Griswold did most of the computer expediting.

To all of the above I express my considerable gratitude.

This work was done under the auspices of the U. S. Atomic Energy Commission.

FOOTNOTES AND REFERENCES

1. Preliminary results on the reaction $K^- + p \rightarrow \Lambda + \pi^0$ were reported by M. L. Stevenson, F. T. Solmitz, C. G. Wohl, and S. G. Wojcicki, Bull. Am. Phys. Soc. 9, 441 (1964), and are included in M. L. Stevenson, Review of Recent Work on K^- Meson Interactions, in Lectures in Theoretical Physics, Vol. VIIB (University of Colorado Press, Boulder, 1965), p. 285.
2. Preliminary results at 1.22 BeV/c were reported by M. Ferro-Luzzi, F. T. Solmitz, and M. L. Stevenson in Proceedings of the 1962 International Conference on High Energy Physics at CERN (CERN, Geneva, 1962), p. 376; preliminary results at 1.42, 1.51, 1.60, and 1.70 BeV/c were reported by C. G. Wohl, F. T. Solmitz, and M. L. Stevenson, Bull. Am. Phys. Soc. 9, 442 (1964). Essentially final results at all momenta were reported by C. G. Wohl, F. T. Solmitz, and M. L. Stevenson, Bull. Am. Phys. Soc. 10, 529 (1965).
3. For a discussion of the assembly line, see A. H. Rosenfeld and W. E. Humphrey, Ann. Rev. Nucl. Sci. 13, 103 (1963).
4. J. Richard Hubbard (Lawrence Radiation Laboratory), private communication, 1964.
5. A. H. Rosenfeld, A. Barbaro-Galtieri, W. H. Barkas, P. L. Bastien, J. Kirz, and M. Roos, Rev. Mod. Phys. 36, 977 (1964). Unless otherwise noted, all physical constants are taken from this reference.
6. Peter G. Wohlmut (Lawrence Radiation Laboratory), private communication, 1965.
7. M. B. Watson, M. Ferro-Luzzi, and R. D. Tripp, Phys. Rev. 131, 2248 (1963).
8. P. L. Bastien and J. P. Berge, Phys. Rev. Letters 10, 188 (1963).
9. C. G. Wohl and S. G. Wojcicki, K^-p Elastic and Charge-Exchange Scattering Around 1.07 BeV/c (Lawrence Radiation Laboratory) unpublished.

10. W. Graziano and S. G. Wojcicki, Phys. Rev. 128, 1868 (1962).
11. W. P. Trower (University of Illinois), private communication, 1965. This is improved over the result reported by W. P. Trower, R. I. Hulsizer, and W. P. Swanson, Some Two Body Final States of K^-p at 1.34 BeV/c, to be published in the Proceedings of the International Conference on High Energy Physics, Dubna, USSR, 1964, but is not final.
12. B. Buschbeck-Czapp, I. Wacek, W. A. Cooper, A. Fridman, E. Malamud, G. Otter, E. Gelsema, and A. Tenner, in Proceedings of the Sienna International Conference on Elementary Particles (Società Italiana di Fisica, Bologna, 1963), p. 166.
13. P. M. Dauber, Phys. Rev. 134, B1370 (1964).
14. P. M. Dauber and H. K. Ticho (UCLA), private communication, 1965; this is a semi-final result.
15. D. Barge, W. Chu, L. Leipuner, R. Crittenden, H. J. Martin, F. Ayer, L. Marshall, A. C. Li, W. Kernan, and M. L. Stevenson, Phys. Rev. Letters 13, 69 (1964).
16. L. Bertanza, V. Brisson, P. L. Connolly, E. L. Hart, I. S. Mittra, G. C. Moneti, R. R. Rau, N. P. Samios, I. O. Skillicorn, S. S. Yamamoto, M. Goldberg, L. Gray, J. Leitner, S. Lichtman, and J. Westgard, in Proceedings of the 1962 International Conference on High Energy Physics at CERN (CERN, Geneva, 1962), p. 284; this is a lower limit.
17. A. Barbaro-Galtieri and R. Tripp, The K^-p Charge-Exchange Reaction at 2.45, 2.63, and 2.70 GeV/c, Lawrence Radiation Laboratory Report UCRL-11429, July 1964 (to be published in the Proceedings of the International Conference on High Energy Physics, Dubna, USSR, 1964); these are preliminary results. The final cross sections will be higher; Frank Shively (Lawrence Radiation Laboratory), private communication, 1965.
18. For a proof of this, see Charles Wohl, Production Angular Distributions, Lawrence Radiation Laboratory Document UCID-2449, August 1964 (unpublished).

19. L. Sodickson, I. Mannelli, D. Frisch, and M. Wahlig, Phys. Rev. 133, B757 (1964) expand some K^-p elastic-scattering differential cross sections both in Legendre polynomial and in cosine power series. A comparison of the two sets of coefficients is instructive; see in particular their Figs. 12 and 13.

20. The modifications fall into the following classes: (a) form factors at the vertices; (b) exchange of Regge poles instead of particles; (c) absorption in the initial and final states. For a discussion of the problems of peripheral models and an introduction to the absorption model, see J. D. Jackson, Rev. Mod. Phys. 37, 484 (1965). The Regge-pole approach is treated by Roger J. N. Phillips and W. Rarita, Regge-Pole Models for High-Energy πN, KN, and $\bar{K}N$ Scattering, Lawrence Radiation Laboratory Report UCRL-16033, April 1965 (submitted to Phys. Rev.).

21. At present there is no elastic-scattering data between 1.4 and 2.0 BeV/c. Little existing data is sensitive to the possible requirement for the higher polynomials in fits with $n_{max} \geqq 6$.

22. For a derivation of the partial-wave equations, see J. Ashkin, Nuovo Cimento 14 Suppl., 221 (1959).

23. J. D. Jackson, Nuovo Cimento 34, 1644 (1964).

24. There can be nonresonant background in the resonant partial wave. It is usually small and neglected; see R. H. Dalitz, Ann. Rev. Nucl. Sci. 13, 339 (1963).

25. Eugene P. Wigner, Phys. Rev. 98, 145 (1955); for a discussion, see Ref. 7.

26. This form was suggested by S. L. Glashow and A. H. Rosenfeld, Phys. Rev. Letters 10, 192 (1963). In a fit to partial widths of baryon resonances, within the framework of SU(3) they found X = 350 MeV. Another prescription, derived nonrelativistically, is given by J. M. Blatt and V. F. Weisskopf, Theoretical Nuclear Physics (John Wiley and Sons, New York, 1952), p. 361. It has the same qualitative behavior as Eq. (16) but, in comparison, requires q^2/X^2 to be greater before $\Gamma \propto q$ prevails. A definitive treatment of barrier effects does not exist.

27. Note that if $\Gamma(\omega)$ increases faster than q^2, at some point above resonance the magnitude of ϵ begins to decrease.

28. At 1.80 and 1.95 BeV/c the expansion coefficients were calculated using the method of moments; thus they are not dependent on a parameter n_{max}.

29. A. Barbaro-Galtieri, A. Hussain, and R. D. Tripp, Phys. Letters 6, 296 (1963).

30. The only data above 3.0 BeV/c are at 9.50 BeV/c; see P. Astbury, G. Finocchiaro, A. Michelini, C. Verkerk, D. Websdale, C. H. West, W. Beusch, B. Gobbi, M. Pepin, M. A. Pouchon, and E. Polgar, Phys. Letters 16, 328 (1965).

31. I am indebted to Robert W. Huff (Lawrence Radiation Laboratory) for derivation and discussion of this result.

32. See, for instance, P. Auvil and C. Lovelace, Nuovo Cimento 33, 473 (1964).

33. This model was first proposed by John H. Munson, K^-p Elastic Scattering at 1.22 BeV/c (Ph. D. Thesis), Lawrence Radiation Laboratory Report UCRL-11155, Dec. 1963 (unpublished). Using considerably less data, he arrived at results practically identical with those found below.

34. W. E. Humphrey, A General Minimizing Routine - MINFUN, Lawrence Radiation Laboratory Alvarez Group Programmer's Note P-6, Sept. 1962 (unpublished).

35. A CERN, Saclay, Heidelberg, Chicago collaboration; Massimiliano Ferro-Luzzi et al. (postdeadline paper), Washington A. P. S. Meeting, April 1965.

36. V. Cook, Bruck Cork, T. F. Hoang, D. Keefe, L. T. Kerth, W. A. Wenzel, and T. F. Zipf, Phys. Rev. 123, 320 (1961).

37. O. Chamberlain, K. M. Crowe, D. Keefe, L. T. Kerth, A. Lemonick, Tin Maung, and T. F. Zipf, Phys. Rev. 125, 1696 (1962).

38. W. A. Blanpied, J. S. Greenberg, V. W. Hughes, P. Kitching, D. C. Lu, and R. C. Minehart, Phys. Rev. Letters 14, 741 (1965).

39. R. K. Böck, W. A. Cooper, B. R. French, J. B. Kinson, R. Levi-Setti, D. Revel, B. Tallini, and S. Zylberajch, A Search for Heavy-Hyperon Resonances Produced by 5.7 GeV/c Anti-protons in Hydrogen (CERN/TC/PHYSICS 65-11), May 1965, submitted to Phys. Letters.

40. Philippe Eberhard, Bull. Am. Phys. Soc. 10, 478 (1965); P. Eberhard and F. T. Shively (Lawrence Radiation Laboratory) private communication, 1965.

41. M. Gell-Mann and Y. Ne'eman, The Eightfold Way (W. A. Benjamin, New York, 1964); this book contains notes by the authors and reprints of 30 papers, including the original (independent) work by the authors.

42. G. F. Chew and S. C. Frautschi, Phys. Rev. Letters 7, 394 (1961); G. F. Chew and S. C. Frautschi, Phys. Rev. Letters 8, 41 (1962).

43. S. Okubo, Prog. Theor. Phys. 27, 949 (1962); reprinted in Ref. 41.

44. J. J. deSwart, Rev. Mod. Phys. 35, 916 (1963); reprinted in Ref. 41.

45. The total width, the πN elasticity, and even the mass of the $N^*_{3/2}(1920)$ are not known accurately, principally because the background in the πN cross sections is quite asymmetric. Auvil and Lovelace (Ref. 32) find the width to be about 175 MeV and the elasticity, x, to be 0.62. (See their Tables III and IV; the "elasticity" of their Table II is the η of our Eq. 10, above.) T. J. Devlin, J. Solomon, and G. Bertsch, Phys. Rev. Letters 14, 1031 (1965), find the width to be about 250 MeV and the elasticity to be 0.57. With a width of 200 MeV and an elasticity of 0.6, $\Gamma(N^*_{3/2}, \pi N)$ is 120 MeV.

46. S. L. Glashow and A. H. Rosenfeld, Phys. Rev. Letters 10, 192 (1963); reprinted in Ref. 41.